CHAPTER 25

Glaciers in China and their variations

Liu Shiyin, Shangguan Donghui, Xu Junli, Wang Xin, Yao Xiaojun, Jiang Zongli, Guo Wanqin, Lu Anxin, Zhang Shiqiang, Ye Baisheng, Li Zhen, Wei Junfeng, and Wu Lizong

ABSTRACT

This chapter summarizes recent glacier variations in China as investigated using remote-sensing methods. We find that glaciers in China have lost a tremendous amount of ice mass since the Little Ice Age maximum: area and ice volume have decreased by 26.7 and 24.5% of the respective amounts of glaciers based on maps compiled during the late 1950s and 1980s. Chinese Glaciers have been in a general state of mass loss during recent decades as monitored by satellite remote-sensing methods over glaciers totaling one fifth of the glacier area in China. At present, the ability to monitor ice volume change and the surface velocity of glaciers by satellite is relatively new, but shows potential for glaciers having complex topographical conditions in the high mountains. This is an important research focus, in part because Chinese economic development is locally heavily impacted by changes in the glacier dynamical regime due to (1) glaciers' role in supplying meltwater to most of the region and (2) potential for local glaciological hazards.

25.1 INTRODUCTION TO GLACIERS IN CHINA

Western China is characterized by numerous mountain ranges and high broad plateaus; 14 mountain ranges run parallel to one another from north to south, including the Altai, Tianshan, Pamirs, Karakoram, Kunlun, and Himalaya, with the latter four ranges surrounding the Qinghai–Xizang (Tibet) Plateau. The mountain ranges of Central Asia host a multitude of glaciers, 46,377 of which are situated within China; they have a total area of 59,425 km^2 based on Chinese glacier inventories (Shi et al. 2005), and account for 52% of the total surface area of glaciers in Asia (Dyurgerov et al. 2002). Statistics show total glacier area and ice volume in the Karakoram, Kunlun, Nyainqentanglha, Himalaya, and Tianshan, account for 78.9 and 84.0%, respectively, of the Chinese total. Of all the glaciers in China, the 77% (by number) that are smaller than 1 km^2 constitute less than 20% of the total area. There are 33 glaciers larger than 100 km^2 in area, with a total area of 6,167 km^2 (10.4% of total area) and an estimated volume of 1,475 km^3 (26.3% of estimated total volume).

Analysis based on observed physical properties, such as ice temperature, surface velocity, and general climatic characteristics over glaciers in various areas in western China, indicates that these glaciers can be categorized into three types: extreme continental, subcontinental, and monsoonal maritime (Shi and Liu 2000). Continental glaciers are mainly located in the middle and western Kunlun Shan, Qiangtang Plateau, eastern Pamirs, western Tanggula Mountains and western Qilian Shan. Subcon-

J. S. Kargel et al. (eds.), *Global Land Ice Measurements from Space*, Springer Praxis Books,
DOI: 10.1007/978-3-540-79818-7_25, © Springer-Verlag Berlin Heidelberg 2014

tinental glaciers are distributed over Tianshan, the northern slopes of the middle and western part of the Himalaya, and the north slope of the Karakoram Mountains. Monsoonal maritime glaciers are mainly located in the southeastern part of the Tibetan Plateau and the Hengduan Mountains in the eastern region of the plateau.

25.2 REGIONAL CONTEXT

As far as precipitation is concerned, the South Asian monsoon and westerlies are dominant in the alpine regions in western China. The vast expanse of the Qinghai–Xizang (Tibet) Plateau (TP) and its high altitude in the interior of the Asian continent contribute to a unique plateau monsoon circulation and, together with local circulation in regional mountains, greatly influences mountain precipitation. The eastern Nyainqentanglha range in southeast Tibet and the Hengduan Mountains enjoy the longest and most abundant rainy season, with annual precipitation of 1,000–3,000 mm at equilibrium line altitudes, creating typical conditions for maritime-type or monsoonal temperate glaciers in China.

In the winter and spring the northern and southern branches of westerlies control the whole TP by creating cold high-pressure zones dominated by clear skies and sparse precipitation, whereas mountains on the western margin of the TP, such as the western section of the Himalaya, Karakoram, western Pamirs, western Tianshan, and Altai Mountains, receive relatively more precipitation. In the summertime, westerlies migrate northward on the TP. The topographical uplift of moisture creates annual precipitation greater than 1,000 mm at the western edge of the Pamirs and the western Karakoram where snowlines are somewhat lowered. Eastward, in the eastern Pamirs and western Kunlun Mountains, annual precipitation drops to only 300–500 mm, and snowline altitudes are much higher than the western Pamirs. The glaciers in the eastern Pamirs and western Kunlun depend on the lower temperatures found in these high-elevation mountains.

The South Asian monsoon also influences the precipitation distribution on the TP and the surrounding mountains. In the wintertime, anticyclones form. In summer, the heating effect over the TP forms strong warm low-pressure zones. Water vapor in this cyclonic circulation condenses and precipitates as rainfall when lifted over the surrounding high mountains, creating rainy belts. Precipitation decreases considerably from the peripheral areas the closer one gets to the TP heartland. Valley wind circulation in mountainous regions also plays an important role in alpine precipitation. Relatively higher levels of rainfall precipitation occur in the alpine zones of the Tianshan, Pamirs, Karakoram, and the Himalaya, second only to the maximum rainfall belt existing at roughly 1,000–2,000 m asl in intervening mountain ranges. However, in the western Qilian, western Kunlun Mountains, and the western TP where water vapor content decreases as aridity rises, glaciers can exist only in favored niches and under the coldest conditions due to lower rates of accumulation (Shi and Bai 1988).

The distribution of rainfall as a result of the annual cycle and timing of high precipitation has more influence on glaciers than the total amount of solid precipitation falling on their surfaces. In the Altai, western Tianshan, Pamirs, and Karakoram Mountains, winter and spring precipitation sourced from Atlantic and Arctic Ocean air currents make up a large percentage of the annual total, while summer precipitation accounts for 40% or less and mostly occurs between May and June (Yang and Zeng 2001). Precipitation in regions far from water vapor sources (such as eastern Tianshan, central Kunlun, Qiangtang Plateau) tends to concentrate in the summer months, resulting in the simultaneous occurrence of glacier accumulation and ablation, and summer accumulation may consequently be much higher than that in winter.

Studying lapse rate patterns and temperature jumps as observed in field investigations, Yang and Zeng (2001) found that the summer mean air temperature during May to August varies between -2.5 and $+4.2^{\circ}$C. Maximum temperatures of 3.9 to 4.2°C occur in mountainous regions with the greatest precipitation in southeastern Tibet, while minimum temperatures of -2.0 to -2.5°C occur in mountainous regions with the least precipitation in the western Kunlun Mountains and Muztag Ata in the eastern Pamirs.

Under steady-state conditions, glacial accumulation at the equilibrium line altitude (ELA) can be represented by points where annual precipitation (p_a, mm) at this altitude is balanced by glacial ablation, which correlates with mean summer temperature (T_{6-8} in $^{\circ}$C) from June to August. It is found that p_a and T_{6-8} at the ELAs of glaciers

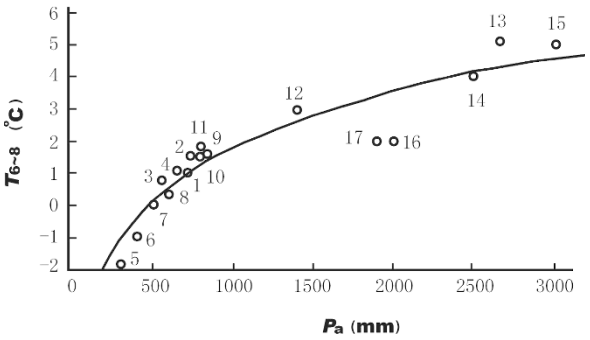

Figure 25.1. The relationship between summer mean temperature (T_{6-8}) and annual precipitation (p_a) at the ELAs of 17 glaciers showing field measurements: 1 = Kanas Glacier in the Altay Mountains; 2 = West Qong Terang Glacier in the Tianshan Mountains; 3 = Glacier U-1 in the Tianshan Mountains; 4 = Sigonghe Glacier No. 5 in the Tianshan Mountains; 5 = Kaltamak Glacier in the Pamirs; 6 = Laohugou Glacier No. 12 in the Qilian Mountains; 7 = Qiyi Glacier in the Qilian Mountains; 8 = Yanglonghe Glacier No. 5 in the Qilian Mountains; 9 = Shuiguanhe Glacier No. 4 in the Qilian Mountains; 10 = Dasuopu (Yebokangjiale) Glacier in the Himalaya; 11 = Rongbuk Glacier in the Himalaya; 12 = Batura Glacier in the Karakoram Mountains (in Pakistani Kashmir); 13 = Ruoguo Glacier in the Nyainqengtanglha range; 14 = Guxiang Glacier in the Nyainqengtanglha range; 15 = Azha Glacier in the Kangri Garpo Range; 16 = Baishuihe Glacier No. 1 in the Hengduan Mountains; 17 = Hailuogou Glacier in the Hengduan Mountains (courtesy of Lai Zuming). Figure can also be viewed as Online Supplement 25.1.

are correlated as follows:

$$T_{6-8} = -15.4 + 2.48 \ln(p_a) \quad (r = 0.94, \alpha = 0.01)$$

This is based on measurements of 16 glaciers in western China and Batura Glacier in Pakistan, as shown in Fig. 25.1. The equation indicates that glaciers in some parts of China mostly depend on cold storage of ice occurring at high elevations, where precipitation is less. For example, where the ELAs of glaciers on the northwestern TP are as high as 5,600–6,000 m asl annual precipitation is 200–300 mm and summer mean temperature is lower than -1°C. Hence, many of these glaciers occur under extreme permafrost conditions.

25.3 METHODS FOR GLACIER CHANGE MONITORING BY REMOTE SENSING

Long-term glacier change detection in China is generally based on results interpreted from remote-sensing data of different periods, mainly detected by applying overlay functions of GIS software. This is facilitated by access to multiple datasets of varying quality, resolution, and precision of production including: (1) previously classified topographic maps (1:50,000 or 1:100,000) derived from aerial photos taken in the 1960s to 1970s; (2) multitemporal Landsat MSS and TM, SPOT, ASTER, and the China Brazil Earth Resources Satellite (CBERS-1) imagery; and (3) ground survey with GPS and geomorphologic mapping. Some assessments are confounded by originally errant photogrammetric or cartographic interpretations, limited local interpretive expertise, variable satellite sensor capabilities, and difficulties of field access.

Depending on the region, different image-processing methods were applied. In some regions, such as the Tarim River basin, all satellite images were geometrically corrected to topographical maps and projected into the Krosovsky spheroid and onto an Albers equal area conic projection; all corrected images were then orthorectified to a digital elevation model (DEM) with 90 m resolution to remove topographical distortions. Errors of geometrical correction are about one pixel, and the error is about 31.5 m for the Landsat TM data determined by randomly selected check points rather than the ground control points used for geometrical correction (Liu et al. 2006). In other regions, such as Muztagh Ata and the Konggur Mountains, glacier outlines from the Chinese Glacier Inventory (CGI) were interpreted and measured by stereo photogrammetry from aerial photos at scales of 1:46,000 to 1:50,000 taken during 1962/1966. They were transferred to topographic maps in the Universal Transverse Mercator (UTM) coordinate system referenced to the World Geodetic System 1984 (WGS 84). The 1981 DEM was produced by digitizing 40 m interval contours and spot heights from the same topographic maps, using ArcView software. Composite images from bands 5, 4, and 3 (30 m resolution) were produced first and merged (pan-sharpened) with a band 8 (15 m resolution) Landsat ETM+ image. These images were orthorectified with the OrthoBASW Generic Pushbroom package using 1:100,000 topographic maps and the 1981 DEM. Twenty independent verification points were selected from each image in order to check co-registration accuracy. The result showed that the residual root-mean-square error (RMSE) of all images was less than 44.9 m (Shangguan et al. 2006).

Different methods have been compared for image classification to extract glacier outlines in China. Compared with other methods, the ratio of TM3/TM5 with a threshold larger than 2.1 gives the best results for the three different types of glaciers (marine, continental, and subcontinental) including within areas subject to slope shadows. Additionally, a Karhunen–Loève (K-L) transform was shown to efficiently enhance the image when classifying debris-covered marine-type glaciers (Shangguan Donghui 2007). However, manual corrections were still needed even under optimal data conditions.

Due to limitations of the method employed, misidentification is frequent. For instance, seasonal snow patches adjacent to glaciers or debris-covered surfaces are difficult to distinguish from bedrock owing to their similar spectral properties. In these cases, manual corrections were applied. Manual delineation was also used to recognize the boundaries of the termini of debris-covered glaciers, a procedure usually based on the geomorphological pattern of the image draped over a DEM.

25.4 GLACIER AREA EXTENT CHANGE

25.4.1 Glacier change since the Little Ice Age maximum

In western China, the most recent cold period to occur happened during the 17th century. This is known from lichenometrical dating of end moraines, ice cores, and tree rings, when glaciers reached their lowest elevations and formed the most easily identified and recent moraines. By using aerial photos acquired during the late 1950s and early 1980s in combination with 1:50,000 and 1:100,000 topographic maps, we can identify and measure the extent of glaciers as they existed during the Little Ice Age maximum (LIAM), including their glacier area, length, and terminus altitude. Ice volume during the LIA can be estimated from the statistical relationship between the volume and area of glaciers ($V = 0.04S^{1.35}$, where V is glacial ice volume in km^3, and S is glacier area in km^2; Liu et al. 2003). Note that this volume–area scaling is close to the scaling exponent of 1.375 found by Bahr et al. (1997) for mountain glaciers. Studies of glacier change since the LIAM began in the 1980s. Wang (1991) measured the LIA glacier extents of over 800 glaciers in the Qilian, Tianshan, Altai, and Kunlun Mountains, as well as the interior of the TP. Su and Shi (2000) surveyed the LIA glacier extents of more than 1,000 glaciers in southeast Tibet. Wang and Ding (2002), Liu et al. (2002, 2003), and Lu et al. (2002) also measured LIA glacier extents in the eastern Tanggula Range, the Anyemagen Range (the source of the Yellow River), the Qilian Mountains, and the Geladaindong area (the source of the Yangtze River). By combining these data with those of 844 recently measured glaciers in the middle and western Himalaya and the inner TP, we have determined the LIA glacier extents of over 3,100 individual glaciers in western China (Fig. 25.2). Of all the measured glaciers, 181 have an area (Fig. 25.2) in excess of 10 km^2, 12 glaciers are larger than 100 km^2, the largest being 252 km^2 as determined during mapping from the 1950s to the 1970s.

Statistical analyses of the abovementioned data (where available) reveal that a linear relationship exists between LIA area (S_{lia}) and that of modern glaciers (S_m), the same applies to LIA ice volume (V_{lia}) and modern ice volume (V_m), and LIA length (L_{lia}) and modern length (L_m), as follows:

$$S_{lia} = 1.0172 \times S_m + 0.3285 \quad (R^2 = 0.99, n = 2{,}409)$$

$$V_{lia} = 1.0161 \times V_m + 0.028 \quad (R^2 = 0.99, n = 2{,}408)$$

$$L_{lia} = 1.0533 \times L_m + 0.3351 \quad (R^2 = 0.98, n = 1{,}372)$$

By means of these equations, we can extrapolate geometrical changes in glaciers in western China since the LIAM without conducting field measurements, and thereby make a general estimate of glacier change since the LIAM as shown in Table 25.1.

Table 25.1 shows that from the time of the LIAM to the middle of the 20th century (1950s through the 1980s), glaciers in western China lost a total area of ~16,013 km^2, or 26.9%. Using volume–area scaling relations, this mass loss corresponds to a total ice volume decrease of 1,373 km^3 (approximately 1,250 Gt assuming ice density of 910 kg/m^3, or ~12.5 Gt yr^{-1} for about 100 years between about 1860 and 1960), almost a quarter of their 1950s to 1980s' total. Glacier mass loss since the LIAM shows obvious regional disparity. Glacial shrinkage demonstrates a radial pattern with the percentage of shrinkage increasing gradually away from the central TP toward its surrounding mountains. For example, regions located far from the interior of the TP, like the southern slopes of the Altai, the Ili River basin, northwestern Tianshan, source areas of the Mekong, Nujiang, and Yangtze Rivers in the Hengduan Mountains, and the lower reaches of the

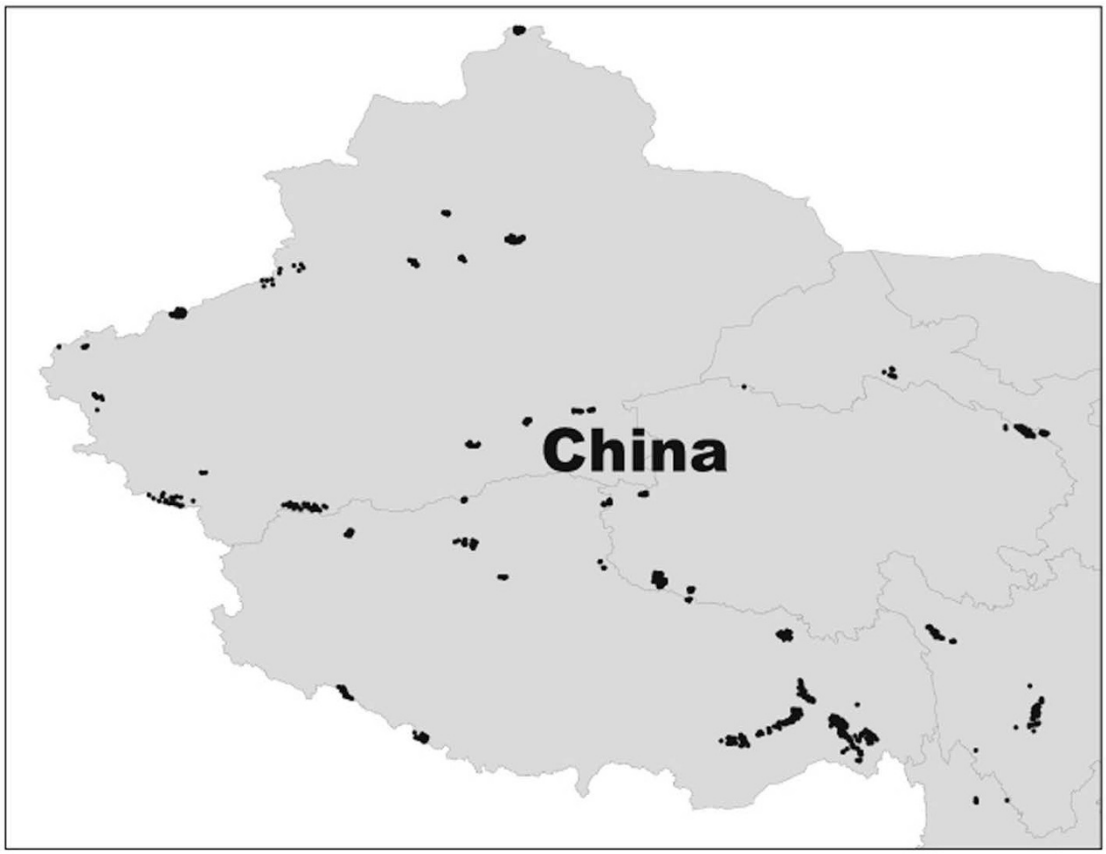

Figure 25.2. Map showing the distribution of glaciers and their LIAM measurements.

Table 25.1. Estimated change in area and volume of glaciers since the LIAM in western China.

River basins	*Glacier count*	*Area decrease since the LIA* (km^2)	*Glacier area decrease* (%)	*Ice volume decrease since the LIA* (km^3)	*Ice volume decrease* (%)
Ob	403	−137.4	−47.5	−11.6	−70.7
Yellow	176	−60.8	−35.3	−5.1	−41.5
Yangtze	1,332	−470.2	−24.8	−39.6	−26.9
Mekong	380	−130.3	−41.2	−10.9	−60.9
Nujiang (Salween)	2,021	−693.7	−40.1	−58.4	−50.8
Ganges	13,008	−4,584.5	−25.3	−389.6	−24.0
Indus	2,033	−692.8	−47.7	−58.4	−62.2
Rivers in arid northwest China	21,683	−7,598.1	−27.5	−651.4	−23.3
Inner region of Tibetan Plateau	5,341	−1,645.4	−21.0	−148.1	−19.0
Total	*46,377*	*−1,6013.2*	*−26.9*	*−1,373.1*	*−24.5*

Yarlung Zangbo River, have lost much more glacier area and ice volume than the central part of the Plateau. Such a regional pattern of glacial shrinkage is closely related to the location of different glacier types and their response sensitivities to climate change.

The above estimation of glacial shrinkage does not include ice loss resulting from the total disappearance of small glaciers since the LIA maximum. A study by Wang and Ding (2002) indicated that about 184 glaciers less than 0.6 km in length might have completely disappeared in the Bujia Kanri region of the eastern Tanggula range since the LIA, accounting for a total glacier area of 24 km^2, roughly half the regional decrease thus far identified. Considering the large percent of small modern glaciers compared with the total in western China, the above estimation of glacial shrinkage could be considerably lower than the actual reduction in area and volume of glaciers since the LIAM. However, since these small disappearing glaciers contain relatively small ice volumes, their role in China-wide or regional total statistics is much more pronounced for area than for volume.

25.4.2 Glacier change during recent decades

Remotely sensed digital images have been widely used to extract information about glacier change during past decades in China (Liu et al. 2002, 2003, 2004, 2005, Lu et al. 2002, Jin et al. 2004, Shangguan et al. 2004a, b). As shown in various papers and in Table 25.2, the date and data type for the extraction of glacier change in different regions differ. For example in the northern Tianshan (China), we used aerial photos taken in 1964 and 1992 for the Urumqi River source area, and in 1962 and 1989 for the Sikeshu River and the Kax River (Liu et al. 2002a). In other regions, Landsat ETM+ images acquired during 2000–2002 were applied for the extraction of recent boundaries of glaciers, while glacier distribution in these regions in the past were mainly based on topographical maps produced by aerial photogrammetric methods, and map revisions based on aerial photos acquired in the late 1950s and early 1980s. The results of recent glacier change studies are shown in Table 25.3.

Table 25.2. Data types used for analyzing glacier change during past decades in selected mountain regions in China (Ding et al. 2006).

Mountain range	*First data acquisition*		*Second data acquisition*	
	Data type	*Dates*	*Data type*	*Dates*
Qilian Shan	1:50,000/100,000 topographic maps, aerial photos	1956, 1966, 1972	Landsat TM	2000, 2001
Tian Shan	1:100,000 topographic maps, aerial photos	1962, 1964	Aerial photos Landsat TM	1992, 1989 1999, 2000
Kunlun Shan	1:100,000 topographic maps, aerial photos	1970, 1966	Landsat MSS Landsat TM/ETM+	1976, 1989 2000
Karakoram	1:50,000/100,000 topographic maps, aerial photos	1937, 1968	Landsat MSS Landsat ETM+	1973 2000
East Pamirs	1:100,000 topographic maps, aerial photos	1962–1965, 1975, 1985	Landsat TM ASTER	2001 2001
Inner TP	1:100,000 topographic maps, aerial photos	1974	Landsat TM	2001
Southeast TP	1:100,000 topographic maps, aerial photos	1980	CBERS, Landsat TM	2001
North slope of Mt. Qomolongma	1:50,000/100,000 topographic maps, aerial photos	1970	ASTER, CBERS	2001, 2002

CBERS = China–Brazil Earth Resources Satellite; Landsat TM = Landsat Thematic Mapper; Landsat ETM + = Landsat Enhanced Thematic Mapper; Landsat MSS = Landsat Multispectral Scanner; ASTER = Advanced Spaceborne Thermal Emission and Reflection Radiometer; TP = Qinghai-Xizang (Tibet) Plateau.

Table 25.3. Glacier change in representative regions in western China during the past few decades monitored by remote sensing (Ding et al. 2006).

Mountain region	*Time span for observations*	*Number of glaciers*	*Glacier area when first measured* (km^2)	*Change in glacier area* ($\pm km^2$)	*Change in glacier area* (%)	*Number of advancing glaciers*
Western Qilian Mountains	1956–1990	170	162.8 ± 3.3	-7.8 ± 0.2	−4.8	0
Tianshan	1962–1964, 1989, 1999, 2000	960	$2{,}382.6 \pm 119.1$	-111.3 ± 0.6	−4.7	224
TP	1966, 1968–1970, 1980–1999, 2000, 2001	2,572	$7{,}282 \pm 218.5$	-236 ± 7.1	−3.2	387
Eastern Pamirs	1960, 1975–1999	753	$1{,}889.7 \pm 94.5$	-188.1 ± 9.4	−10.0	198
Karakoram	1968–1999	565	$2{,}707.3 \pm 243.7$	-111.1 ± 10	−4.1	85
Total		*5,020*	*$14{,}424.4 \pm 679$*	*-654.3 ± 27.2*	*−4.5*	*894*

25.4.2.1 Qilian Shan

There are 2,815 glaciers covering a total area of 1,931 km^2 with an ice volume of ~93 km^3 in the Qilian Shan. Most glaciers (69% of the area total) occur on the northern slopes of the mountain. Laohugou No. 12 Glacier is the largest valley glacier, being 10 km in length and 21.9 km^2 in area. The Dunde Ice Cap is the largest flat-topped ice mass and has an area of 57.07 km^2.

Comparison of glacier termini from Landsat TM images acquired in 2000 and 2001 and aerial photos taken in 1956, 1966, and 1972 indicated that the 33 glaciers monitored on the northeastern slope of the eastern end of the mountains were all receding, at a mean length reduction rate of 11.5 m yr^{-1}. Six glaciers completely disappeared between 1972 and 2001. In the western section of the mountains, 95% of monitored glaciers retreated at a mean rate of 4.9 m yr^{-1}, but we determined that 10 glaciers advanced between 1956 and 2000/2001. Our analysis indicated that about 170 glaciers monitored on the northwestern slope of the western section lost 4.8% of their total area during the period 1956–1990, with a far greater area reduction (23%) for small glaciers ($\leq$1 km^2) (Liu et al. 2003).

25.4.2.2 Tianshan

There are ~9,000 glaciers covering a total area of 9,225 km^2 in the Chinese Tianshan. Six glaciers around the Mt. Tomur–Khan Tengri massif are larger than 100 km^2, with Tomur Glacier being the largest with an area of 338 km^2. These large glaciers are termed Turkestan-type glaciers (valley glaciers without névé basins fed by ice slides and avalanches) and have widespread supraglacial debris cover and thermokarst geomorphology on the ablation area. Considering the mean area of glaciers in Tianshan and the important nourishment supply of river runoff, these large glaciers play a key role in surface water resource variation in this arid region.

Repeat photogrammetric mapping from two acquisitions of aerial photos has been carried out for measurement of glacier variation in the Urumqi River basin (1962 and 1992) and source tributaries of the Yili River basin (1962 and 1989) on the northern slopes of the Tianshan Mountains. All the 251 glaciers within the study retreated during the periods indicated above, but overall area reduction differed significantly between the two basins: 13.8% in the Urumqi River basin, but only 3.1% in the Yili River basin. However, estimated ice volume change indicates that the average thickness of glaciers after thinning is similar for the two basins: 5.8 m for the Urumqi and 6.1 m for the Yili (Liu et al. 2002a). As far as glacier change on the southern slopes of the Tianshan Mountains is concerned, our analysis based on comparison of aerial photos taken in the early 1960s with Landsat TM images in 1999 and 2000 shows that 69.4% of monitored glaciers have receded and 30.4% have advanced during the past 40 years. Subtracting the area

increase from the advance of some monitored glaciers covering a total area of 2,093.8 km^2 in the early 1960s, glaciers in the southern Tianshan still lost 4.6% of their area.

25.4.2.3 Eastern Pamir Plateau

China's eastern Pamir Plateau (38–39°N, 74°40′–75°40′E) is located at the western end of the Tarim Basin. The Plateau is above 3,000 m asl and Mt. Konggur (7,719 m asl) is its highest peak. According to the Chinese Glacier Inventory (CGI) (Yang and An 1989, Liu et al. 2001), the Plateau is home to 1,277 glaciers covering a total area of 2,670.61 km^2.

Change in 880 of the glaciers in the eastern Pamir Plateau were monitored using aerial photos taken in 1962–1966, Landsat TM in 1990, and Landsat ETM+ in 1999. The results indicated that these glaciers have lost a total of 173.26 km^2, 7.9% of that in 1962–1966, mainly due to changes observed in 1990–1999, when annual area loss almost tripled to 1.01 $km^2\ yr^{-1}$ from the annual rate in 1962/1966–1990. Mean frontal retreat of glaciers in the Muztagh Ata and Konggur Mountains increased from 6.0 m yr^{-1} between 1962–1966 and 1990 to 11.2 m yr^{-1} between 1990 and 1999, with overall glacier length reduction of 9.9% for the whole study period. Loss of glacier area in the region was mainly contributed by glaciers smaller than 5 km^2 in size (i.e., 82.0% of total area loss; Shangguan et al., 2006). This indicates that small glaciers are generally more sensitive to climate change than large glaciers. Some glaciers ran counter to this, however, and showed an area increase throughout the period. The mean size of glaciers in the Muztagh Ata and Konggur Mountains decreased from 2.56 to 2.38 km^2 between 1962 and 1999. It was found that three glaciers (CN5Y663B17, CN5Y662D25 and CN5Y662F1 according to their WGMS IDs) have disappeared. The most obvious area reduction was found at CN5Y663D99 which had an area of 17.23 km^2 in 1962; it lost 3.13 km^2 of ice between 1962 and 1990 and 0.24 km^2 between 1990 and 1999. This glacier shows that retreat in the region accelerated from the 1990s. As a whole, glacier area shrank by 3.37 km^2, some 19.6% of its 1962 area.

25.4.2.4 Karakoram

The northern slopes of the Karakoram are among the most highly glacierized areas in China, and home to K2, the second highest mountain peak in the world. Early research from *in situ* observations in 1937, topographic maps in 1968, and a Landsat MSS image in 1973 show that K2's Qoger Glacier retreated by 1.7 km between 1937 and 1968 but the retreat slowed between 1968 and 1973. Similar changes occurred in two nearby glaciers, but two advancing glaciers were found in the region during the same period (Zhang, 1980). Careful analysis based on maps and Landsat ETM+ imagery indicates that glacier change in this region is complicated. Some large glaciers were in steady state (equilibrium), have advanced, or even surged during recent decades (Shangguan et al. 2004b). Glacier mass in recent years has generally increased (Gardelle et al. 2012).

25.4.2.5 Tibetan Plateau

The broad area and regional high elevation of the TP provide optimum conditions for the development of glaciers under present-day climatic conditions. Glaciers on the TP account for 84 and 81.6%, respectively, of the total area and volume of glaciers (including those in the Karakoram and Qilian Shan) in China. As a result of complex meteorological factors brought about by westerlies and the South Asian monsoon, glaciers on the TP are of monsoonal maritime type (temperate southeastern part and Hengduan Shan), of subcontinental type (Himalaya, central northeast part), and of extreme continental type (central and northwest part). Glacier change in the TP reflects differing patterns of climate in different parts of this large region. Glaciers in the Kunlun Shan, a mountain range along the northern margin of the TP, which extends from west to east, have generally retreated during the past four decades. However, the reduction in glacier area is larger (17%) at the eastern end of the mountains (1966 baseline; Liu et al. 2002b) compared with that (0.3%) at the western end (1970 baseline; Shangguan et al. 2004a), with intermediate changes in the central section (Liu et al. 2004). In the central part of the TP, glaciers have been in relative equilibrium but show a trend toward general retreat during the past three decades (e.g., a decrease of 1.7% in glacier area in the basin in which the source of the Yangtze River is located; Lu et al. 2002). However, glaciers on the northern slopes of the Himalaya have experienced extensive wastage as indicated by Jin et al. (2004); many small glaciers may have actually disappeared during the last 20 years.

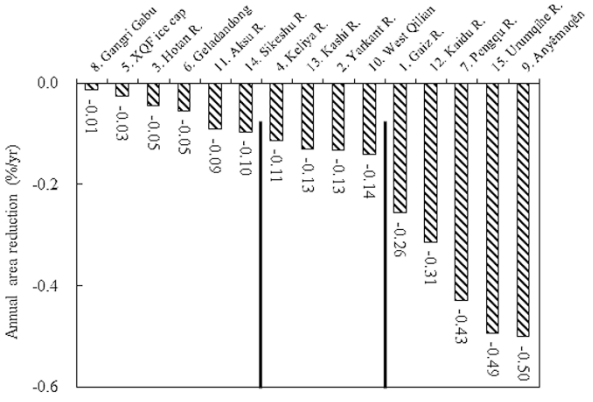

Figure 25.3. Annual percentage glacier area change in each river basin and mountain range. Figure can also be viewed as Online Supplement 25.2.

Change in monsoonal maritime glaciers in the southeast TP (e.g., the Gangrigabu Mountains) shows a particularly interesting pattern (Liu et al. 2006). The mountains are located at the eastern end of the Nyainqentanglha Mountains, which run about 280 km from northwest to southeast. Through this region flows a tributary of the Yalung Zangbu River, one of the upper basins of the Brahmaputra. There are 1,320 glaciers in the range, with a total area and volume of 2,655.2 km^2 and 260.3 km^3, respectively, according to the Chinese Glacier Inventory (CGI) (Mi et al. 2002). From aerial photos taken in October 1980 two topographic maps were made: one a 19 m resolution CBERS image acquired on January 30, 2001 and the other a 30 m resolution Landsat TM image taken on October 26, 1999. This showed that the 88 monitored glaciers (covering a total area of 444.6 km^2) lost only 2 km^2. The reason for this was that 60% of this area's glaciers were in retreat, whereas other glaciers were advancing at the same time (1980–2001). As argued by Su and Shi (2000), their measurements of 245 glaciers in the drainage area of the Zayu (or Chayu) River on the southern slopes of the range had lost 36.9% of their area between 1915 and 1980. Although these glaciers are very small, averaging only 1.41 km^2, this confirms the fact that glaciers in the region are sensitive to climate change. The advance of many glaciers during the past two decades may confirm the changing pattern of glaciers in the southeastern TP under temperate conditions.

25.4.2.6 Integration

By integrating the results of glacier change in western China during the past 50 years, we conclude that 82.2% of all monitored glaciers were in retreat, while the remaining glaciers were advancing with some surging (Ding et al. 2006). This does not necessarily mean that such glaciers advanced over the entire observational period. Many may now be in retreat despite earlier expansion as regional climate warming has been much more evident since the 1980s than in earlier decades. Even compensating for the increase in area of some glaciers, those that have been monitored still show total area loss of 4.5% from the late 1950s to the late 1970s (Table 25.3). As reflected by mass balance variations on Glacier No. 1 and other representative glaciers, mass wastage has tended to accelerate since the late 1970s or early 1980s, and especially so during the 1990s.

As can be seen in Table 25.3, the period of observation of glacier change differs for the regions considered here. This is due to differences in the acquisition times of aerial photos and satellite images. To examine the regional characteristics of glacier change, we calculated annual percentage glacier area change (henceforth APAC) in every river basin or mountain region, as shown in Fig. 25.3. Of the 15 glacierized basins or mountain regions monitored, APAC shows large regional differences that can be classified into three groups: Class A ($APAC \leq 0.1\%/yr$, regions 3, 5, 6, 8, 14); Class B ($0.1\% < APAC \leq 0.2\%$, regions 2, 4, 10); and Class C ($APAC > 0.2\%$, regions 1, 7, 9, 12, 15). These regional differences in glacier area reduction may arise from a combination of differences in (1) monitoring period, (2) regional climate change, and (3) individual glacier responses to such change.

25.5 CHANGE IN SURFACE ELEVATIONS

25.5.1 Koxkar Glacier

Use of the various techniques available to monitor change in glacier surface elevations has not been widely carried out in China. Such an attempt, however, was done on Koxkar Glacier (CN5Y674A5, 41°48.77′N, 80°10.20′E; Fig. 25.4) located on the southern slope of Mt. Tomur, Tianshan. The glacier is 83.56 km^2 in area, 26.0 km in length, and has an ablation area of 30.6 km^2 that is mostly covered by debris. In the study, ice surface elevation change was measured on the ablation area below 4,200 m.

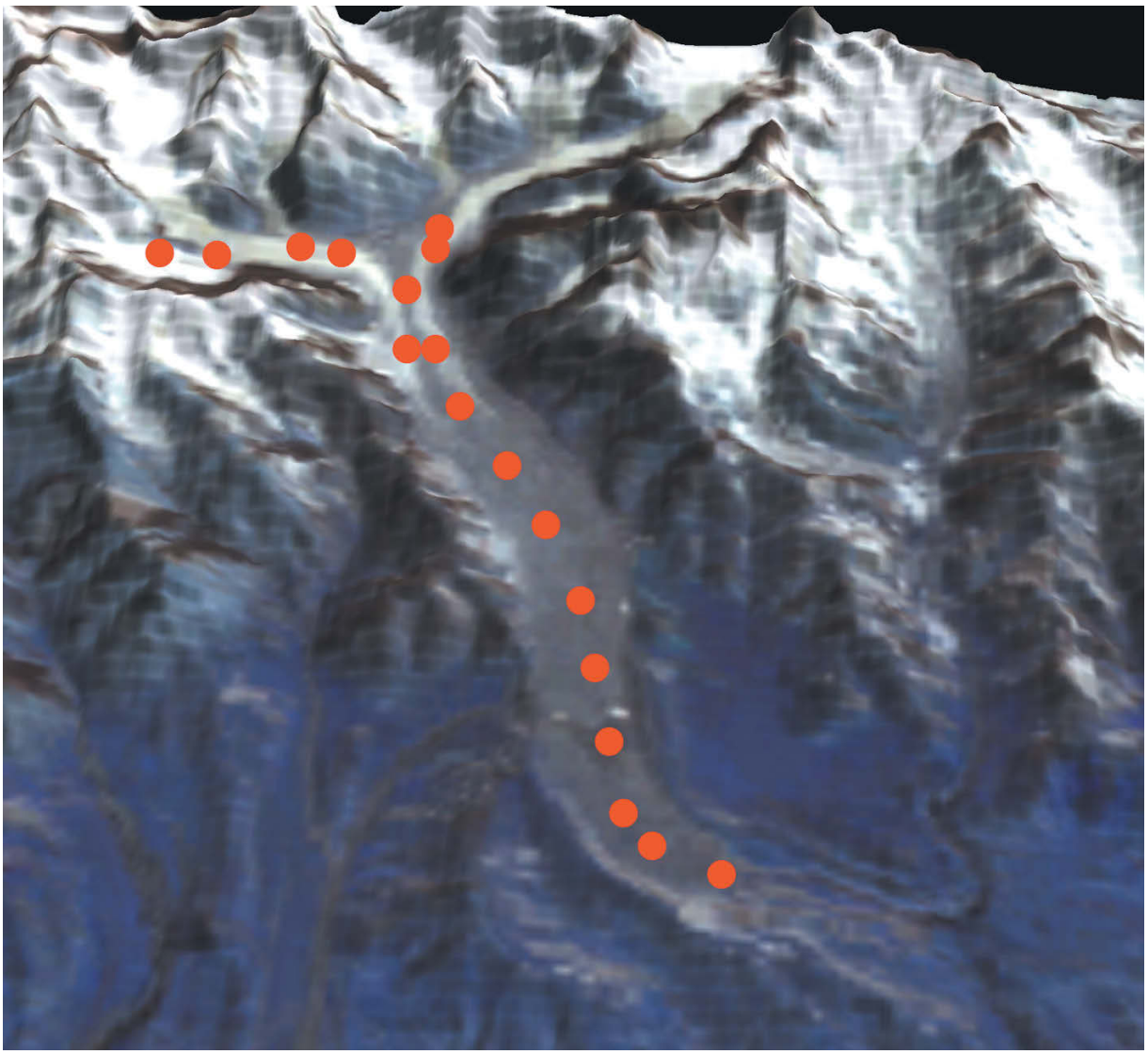

Figure 25.4. 3D view of Koxkar Glacier on the south slope of Mt. Tomur, Tianshan. The ASTER image is draped over a 30 m resolution DEM. Red dots are ablation stakes installed during 2003 and 2005.

In this study, we have used data from: (1) a DEM made from 1:50,000 topographical maps of 1974 (DEM1974); (2) stereo pairs of ASTER images acquired on October 31, 2000; (3) ground control point measurements by SOKKIA GSSIA differential GPS in May 2004; (4) measurements of 18 ablation stakes during the period 2003–2005. A GPS survey was completed for 168 ground control points spaced ~150 m apart on the glacier. A DEM made from ASTER image pairs (DEM2000) was generated (Kääb et al. 2003, Hirano et al. 2003). The DEM2000 and GPS point survey data were reprojected into the same coordinate system as the DEM1974 (Beijing 54 coordinate system, Huanghai vertical datum 1956) from UTM WGS 84 by means of a seven-parameter transformation model (Wang et al. 2003b).

Obvious errors were found in DEM2000 in accumulation areas higher than 4,400 m due to the influence of snow cover. Therefore, DEM2000 could only be verified in the region below 4,200 m. Comparing elevations produced by DEM1974 and DEM2000 along a profile in a nonglacierized area near the glacier, we found that the mean vertical error of DEM2000 is about ±35.7 m, with a maximum of 89 m. In case DEM1974 also had

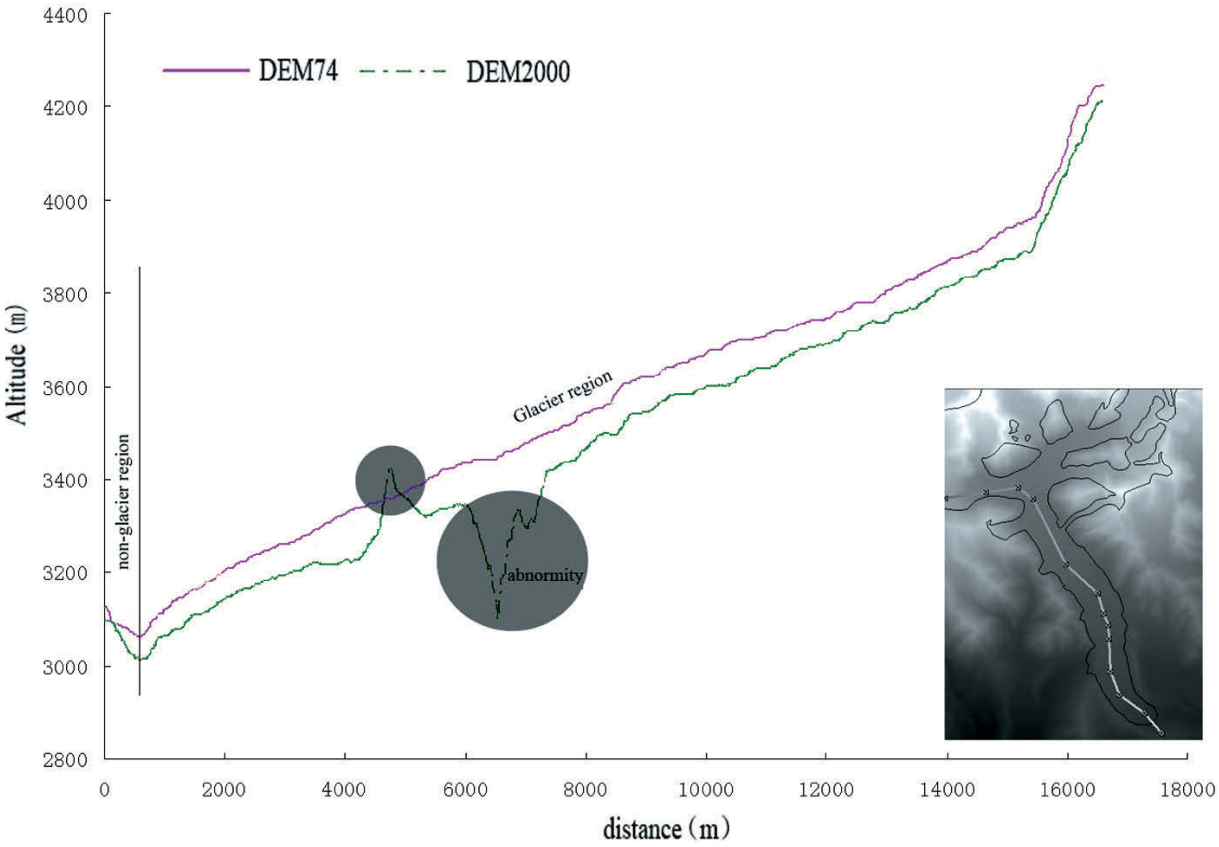

Figure 25.5. Comparison of elevation profiles of DEM1974 and DEM2000 along the central flowline (inset DEM) of Koxkar Glacier.

errors, we checked the elevation difference of DEM1974 by GPS measurements at two survey ground control points in the region. The results revealed that differences are within ±26 m.

By comparing DEM1974 and DEM2000, we found that elevations of the glacier surface below 4,200 m thinned by an average of 69.6 ± 35.7 m between 1974 and 2000, or 2.7 ± 1.4 m yr^{-1}. Along the central flowline of the ablation area (Fig. 25.5), an obvious lowering of surface area of between 3,300–3,500 m occurred on the glacier. Above 3,900 m, surface lowering decreased as elevation increased. Compared with GPS measurements, average surface lowering on the ablation area was 68.4 ± 26 m or 2.3 ± 0.87 m yr^{-1} between 1974 and 2004. Putting the influence of ice mass transfer to one side, the above results are comparable with the ablation measurements collected at the stakes below 4,200 m on the glacier during 2003–2005 (e.g., melting rates were 2.1–2.4 m yr^{-1}; Zhang et al. 2006a). This point suggests that mass transfer by flow was much smaller than ablation and thinning.

25.5.2 Yanglong River

Yanglanghe Glacier No. 1 (CN5Y432A1, YLHG1, 39°13′00″N, 98°33′00″E) and No. 5 (CN5Y432A5, YLHG5) are located on the north slope of the Suzhulian Peak in the central Qilian Mountains, with total areas of 4.44 and 1.70 km^2 as well as total lengths of 5.1 and 2.5 km in 1956, respectively (Fig. 25.6).

The data used in this research included (1) 1956 aerial photos at a scale of 1:50,000 acquired by the Chinese Military Geodetic Service; (2) 1977 aerial photos at a scale of 1:16,000 acquired by the Cold and Arid Regions Environmental and Engineering Research Institute (CAREERI); and (3) GPS data collected in 2007.

Aerial photos were scanned, georeferenced, and orthorectified using a kilometer grid extracted from a topographic map. The digital elevation models for 1956 (DEM1956) and 1977 (DEM1977) were produced by digitizing 20 and 5 m interval contours and spot heights from topographic maps, respec-

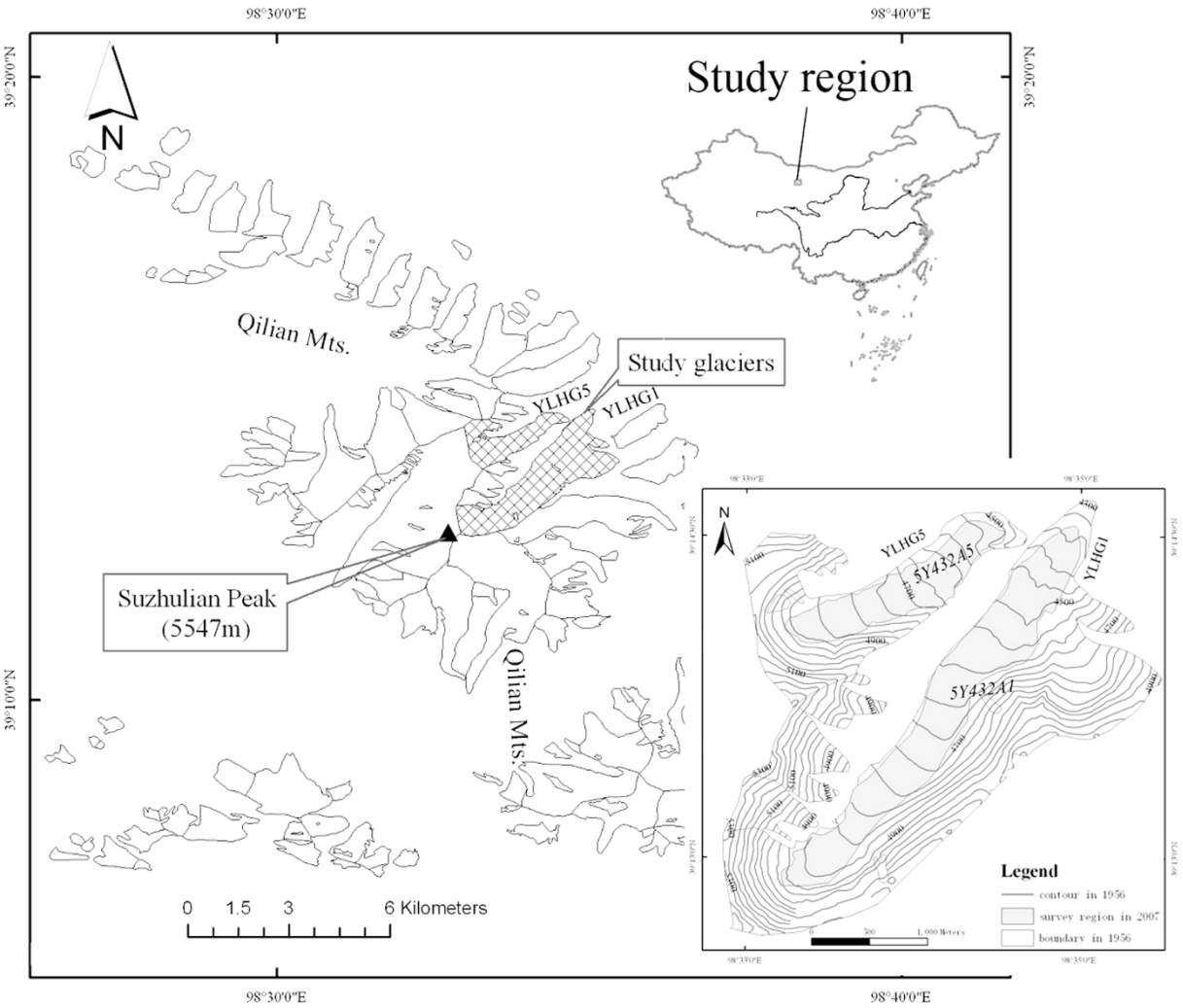

Figure 25.6. A map of YLHG1 and YLHG5 and their surroundings. Figure can also be viewed as Online Supplement 25.3.

tively, interpolated, and put through a 30 m cell size filter, using ArcMap software. The coordinates of both maps are expressed as Beijing 54 (BJ54), Yellow Sea mean sea level (geoid) at Qingdao Tidal Observatory in 1956.

Fieldwork was carried out on YLHG1 and YLHG5 between August 13 and 15, 2007. Five Unistrong E650 dual-frequency GPS receivers were used for kinematic survey. Surface topography points (survey extent is shown in Fig. 25.6) were obtained in RTK mode, in which four receivers were carried by four walkers. Another receiver was installed on a rock outcrop approximately 5 km from a reference station. All the GPS measurements were carried out in ice areas, with distances between kinematic and base measurements no greater than 5 km. The sampling interval was 25–50 m. However, areas of steep ice cliffs were not surveyed due to dangerous walking conditions. Thus, the survey work on YLHG1 and YLHG5 took place in the glacier valleys, which cover total areas of about $4 * 0.36 = 1.44$ and $2 * 0.32 = 0.64$ km^2 (Fig. 25.6) or 32.4 and 37.6% of the total area occupied by the glaciers in 1956, respectively. Data from 837 and 615 topographic points in YLHG1 and YLHG5 were collected, respectively. All GPS data were processed using LandTop 2.0.5.1 software. These data are presented in UTM WGS 84 format.

The projection ellipsoid parameters of BJ54 (center and flattening) are different from those of UTM WGS 84. Therefore, four national trigonometric reference points in BJ54 coordinates were selected to calculate coordinate conversion param-

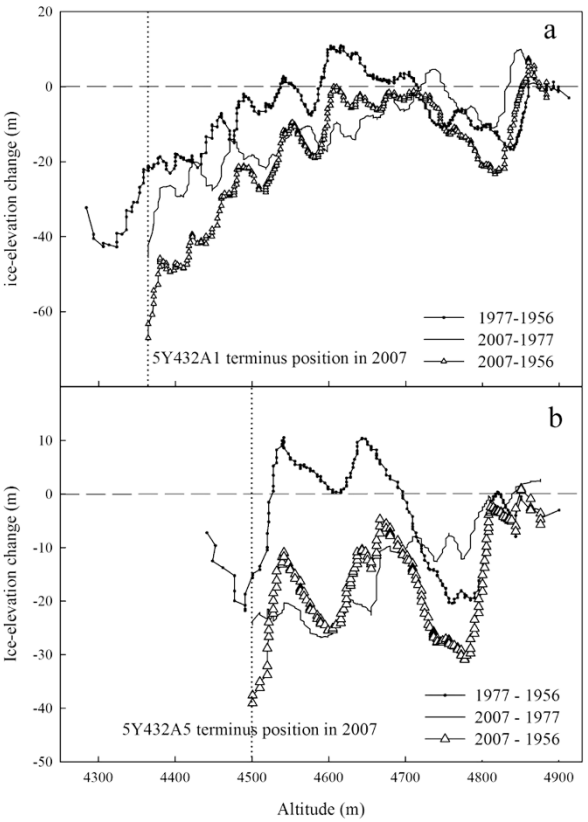

Figure 25.7. Ice elevation change as a function of altitude on 5Y432A1 (a) and 5Y432A5 (b) from topographic maps (1956, 1977) and GPS RTK DEMs (2007). Figure can also be viewed as Online Supplement 25.4.

eters using a seven-parameter model in the space transform through GPS static survey (Wang et al. 2003b). Thus, all data from GPS measurements were reprojected and transformed to BJ54 from UTM WG S84.

When DEM2007 and DEM1956 were compared, we observed strong thinning on the lower parts (altitude less than 4,600 m) of both glaciers (Fig. 25.7). However, despite ice elevation decreasing by about 10–20 m between 4,610 and 4,710 m asl for glacier 5Y432A1 and between 4,630 and 4,670 m asl for glacier 5Y432A5, there were no significant elevation changes above 4,870 m for 5Y432A1 and 4,820m for 5Y432A5. Fig. 25.8 shows all measured changes in ice elevation from 1956 to 2007. The area undergoing most ice thinning was a pit in glacier 5Y432A1, where the maximum rates of thinning were 1.8 m yr^{-1} between 1956 and 2007 (Fig. 25.8).

Ice thinning was observed to be greatest at the frontal tongues of both glaciers, where the maximum rates of thinning for 5Y432A1 and 5Y432A5 were 1.8 and 0.8 m yr^{-1}, respectively, between 1956 and 2007.

When the two periods are considered separately (by including DEM1977), thinning at low elevations is still present. The data show thinning for both glaciers between 1977 and 2007. However, from 4,585 to 4,710 m asl for 5Y432A1 and from 4,550 to 4,700 m asl for 5Y432A5, the data suggest thickening of 1–10 m between 1956 and 1977 and thinning above 4,710 m for 5Y432A1 and above 4,700 m for 5Y432A5.

Table 25.4 shows change in mean ice elevation and volume between DEM1956, DEM1977, and DEM2007. The results show ice elevation at both glaciers lowering more rapidly in recent years. Between 1956 and 2007, the ablation areas of 5Y432A1 and 5Y432A5 lost ice volumes of about $2.91 * 10^7$ and $1.08 * 10^7$ m^3, respectively, corresponding to mean thickness decreases of 20.2 ± 11 and 16.9 ± 11 m, which represent rates of 0.40 ± 0.22 and 0.33 ± 0.22 m yr^{-1}, respectively. Thus, 5Y432A1 lost 2.7 times the ice volume lost by 5Y432A5. However, these ice volumes exclude those parts of the glaciers lost due to retreat of the terminus; furthermore, elevation changes were not determined for the accumulation areas of the glaciers. The values shown in Table 25.4 are thus smaller than actual changes.

Considering the two periods separately (by including DEM1977), the ablation areas of 5Y432A1 and 5Y432A5 lost ice volumes of about $(0.98 \pm 1.35) * 10^7$ and $(0.12 \pm 0.55) * 10^7$ m^3 between 1956 and 1977, corresponding to mean decreases in thickness of 6.8 ± 11 and 1.8 ± 11 m, which represent rates of 0.32 ± 0.52 and 0.09 ± 0.52 m yr^{-1}, all respectively. The two glaciers (5Y432A1 and 5Y432A5) decreased in volume by $(1.83 \pm 0.27) * 10^7$ and $(1.00 \pm 0.12) * 10^7$ m^3 between 1977 and 2007, corresponding to total decreases in ice elevation of 12.7 ± 2 and 15.7 ± 2 m, respectively, which represent rates of 0.42 ± 0.06 and 0.52 ± 0.06 m yr^{-1}, respectively. Thus, the rates of thinning of both glaciers are increasing, and especially so for 5Y432A5.

25.6 SURFACE MOVEMENT DERIVED BY SATELLITE REMOTE SENSING

25.6.1 Justification

Glacier flow velocity has typically been monitored by measurements taken from a stake network set

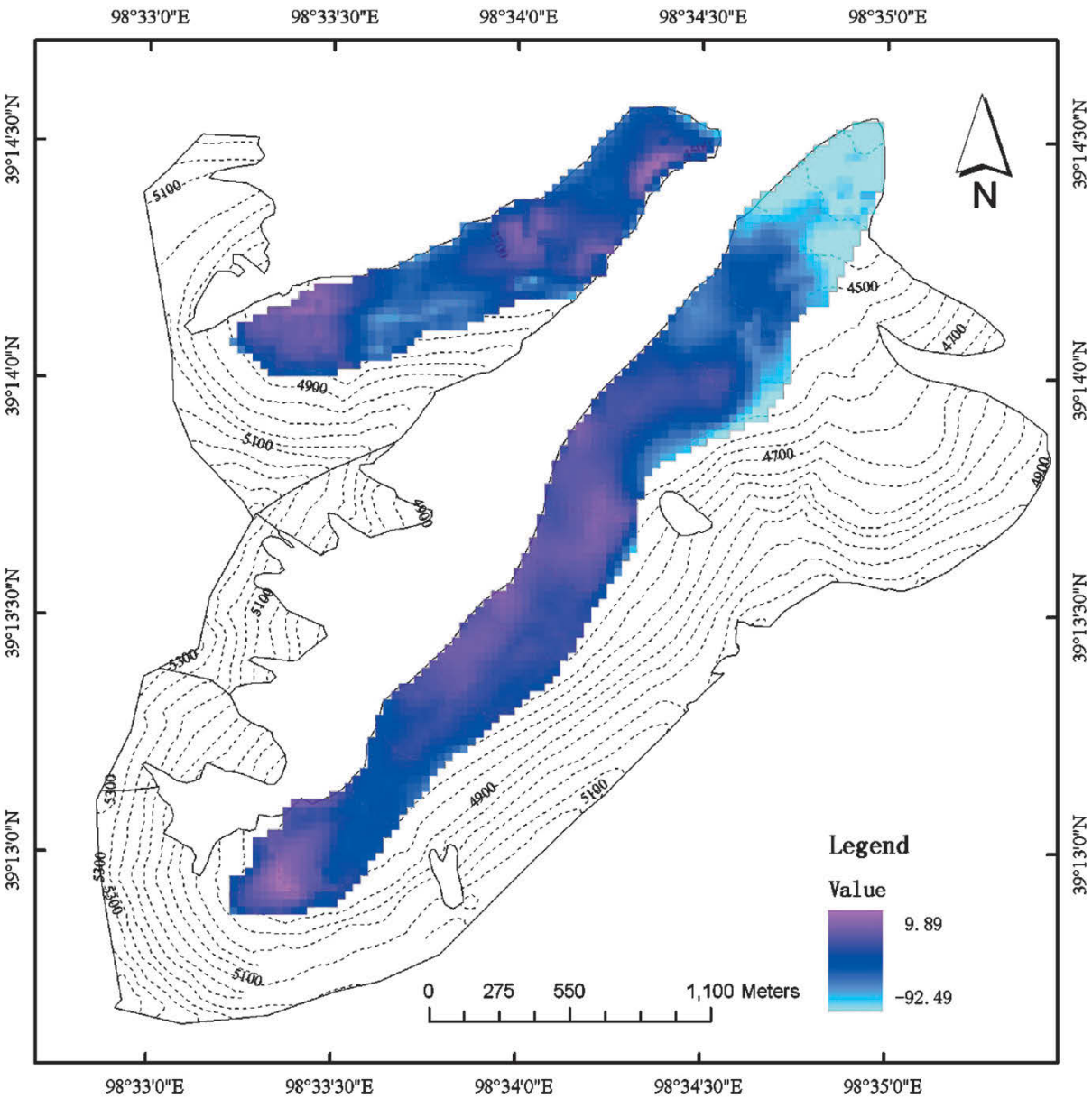

Figure 25.8. The effect of surface elevation change on ablation of YLHG1 and YLHG5 from 1956 to 2007. The largest decrease in ice elevation (92.49 m) was at a pit in 5Y432A1. Line a and b show the routes followed in Fig. 25.7a and Fig. 25.7b, respectively. Map elevation change scale is in vertical meters.

up on the ice surface. Modern techniques such as the differential global positioning system (DGPS), synthetic aperture radar interferometry (InSAR), and optical image cross-correlation have been developed to determine glacier displacements (Berthier et al. 2005). Using DGPS for ice movement measurements is accurate, but laborious and expensive to apply in distant glacierized regions. InSAR is widely used because of its precision, but it too has limitations in mountain glacier areas and requires suitable baseline SAR images with a rigid time interval (Luckman et al. 2007). Compared with the above methods, optical image cross-correlation may be less constrained by topography and data source availability. However, the surface features of glaciers must be obvious in at least two of the repeat images, and it is the spatial resolution of optical images that directly determines

the precision of velocity measurements (Kääb 2005).

In this section, we will show our findings regarding glacier surface displacement by using two approaches: repeat two-pass D-InSAR (differential SAR interferometry) and optical image cross-correlation.

25.6.2 Glacier velocity derived using D-InSAR and SAR feature-tracking methods

Two synthetic aperture radar (SAR) images acquired from two slightly different positions, at different revisit times, are used to measure phase difference, or the so-called interferogram (Zebker et al. 1994). D-InSAR is a widely used method to derive land surface deformation. This technology can be used to extract glacier surface velocity at centimeter or subcentimeter scales (Joughin et al. 1996). Some studies on TP glaciers, such as estimation of Dongkemadi Glacier surface velocities, have used ERS1/2 or ALOS PALSAR data interferometry (Zhou et al. 2009b, Zhou and Li 2011).

Two L-band SAR images covering Dongkemadi Glacier, which is located in the Yangtze River source area of the TP, were acquired by the ALOS/PALSAR system of JAXA during a time span of 46 days with a 265 m perpendicular baseline. Data acquisitions took place on December 10, 2007 and January 25, 2008. The average surface velocity of the glacier derived from this method is about 3 m yr^{-1} (Fig. 25.9).

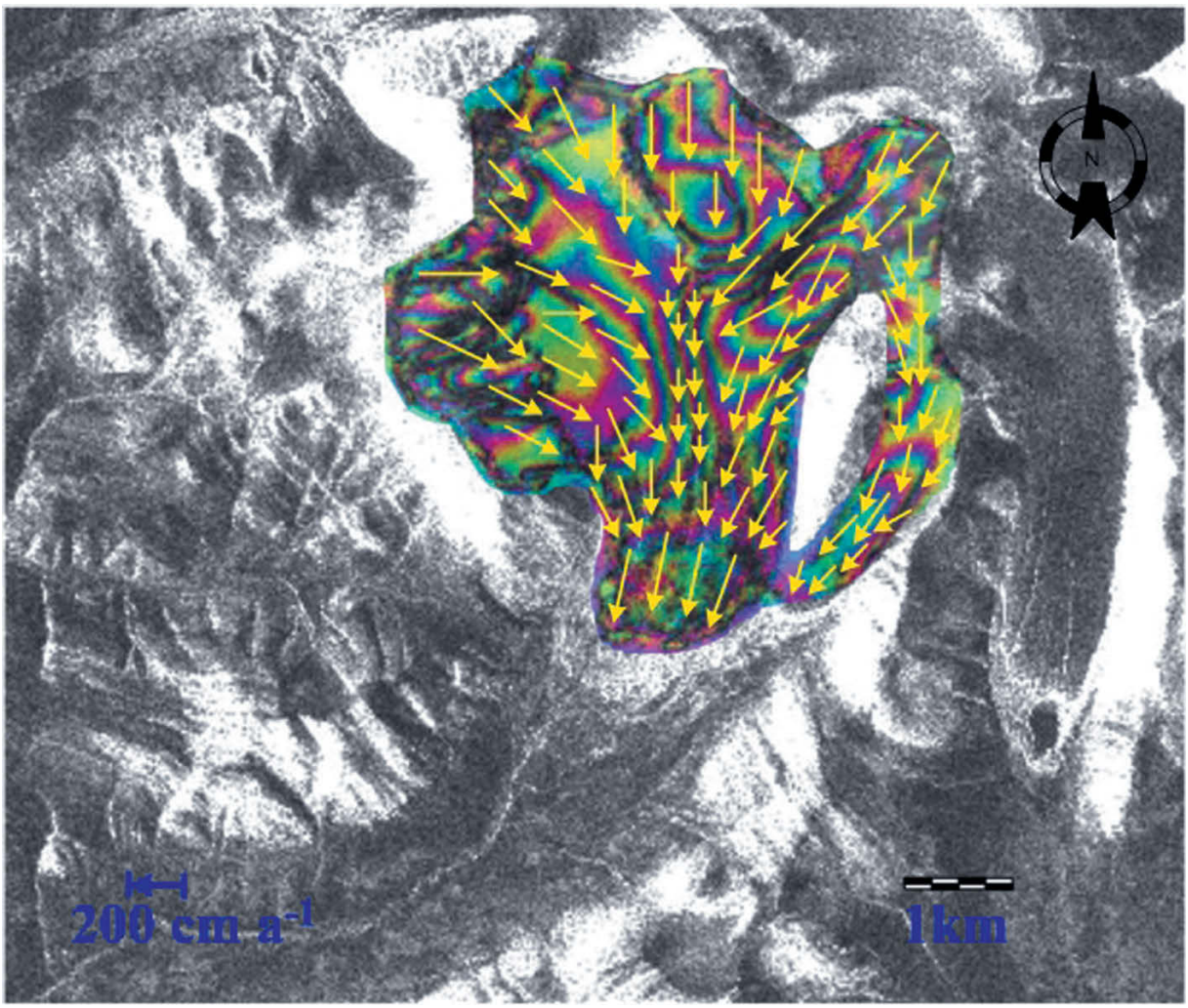

Figure 25.9. The flow field on Dongkemadi Glacier derived by ERS 1/2 D-InSAR.

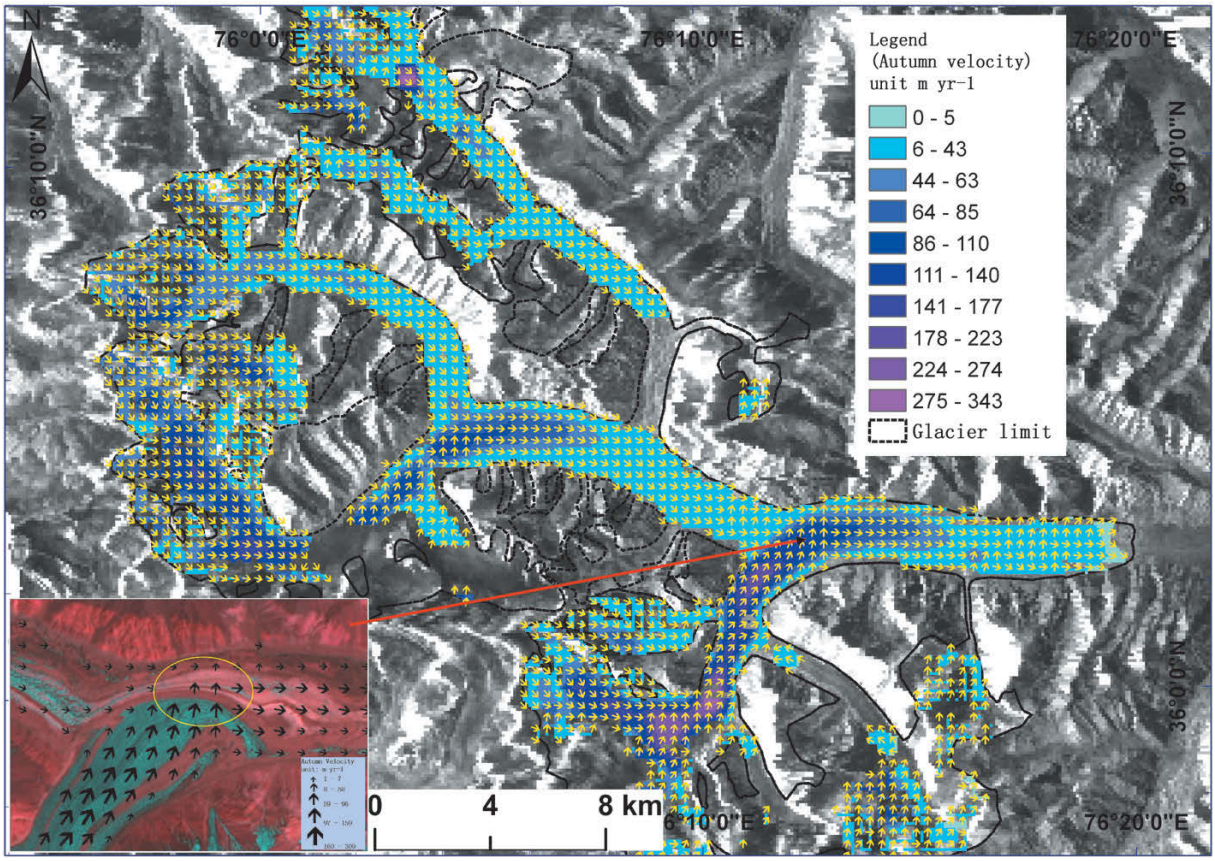

Figure 25.10. Yengisogat Glacier surface velocities from feature tracking of ALOS PALSAR data, Karakoram, China.

Another new method, CR-D-InSAR (corner reflector differential interferometry) was employed to measure surface velocity on the same glacier. Four fast-moving blocks of the glacier were clearly seen (Zhou and Li 2011). This method is more accurate than the conventional version, D-InSAR, and the naturally persistent scatterers method.

The SAR feature-tracking (SRFT) technique can be used to retrieve glacier surface velocities when SAR interferometry is hampered due to the lack of coherence typical of long-time observing intervals of satellites. Feature-tracking of ALOS PALSAR data was used to estimate the surface velocities of several mountain glaciers, such as Yengisogat and Koxkar Glacier (Jiang et al. 2011a).

The seasonal surface velocities of Yengisogat Glacier were measured by means of ALOS PALSAR data feature tracking using GAMMA software. As shown in Fig. 25.10, the southern tributary was moving faster than any other tributaries and was still pushing the glacier trunk. This may imply surging at the southern tributary glacier (Jiang et al. 2011b).

25.6.3 Glacier velocity derived by optical images

Two or more orthorectified satellite optical images from different times were selected for an experiment involving glacier motion measurements. Correlation coefficients were calculated by means of a moving window algorithm with one image as the reference and the other the search image. Chip pixels with a high correlation coefficient on the search image were identified and position differences were calculated from the reference chip's geometry. By moving the search window over the whole glacier, we estimated the surface velocity field of the glacier. Because velocities are computed from orthorectified images, they are plane velocities. The real velocity should be corrected by taking topography into account, which can be done with a DEM.

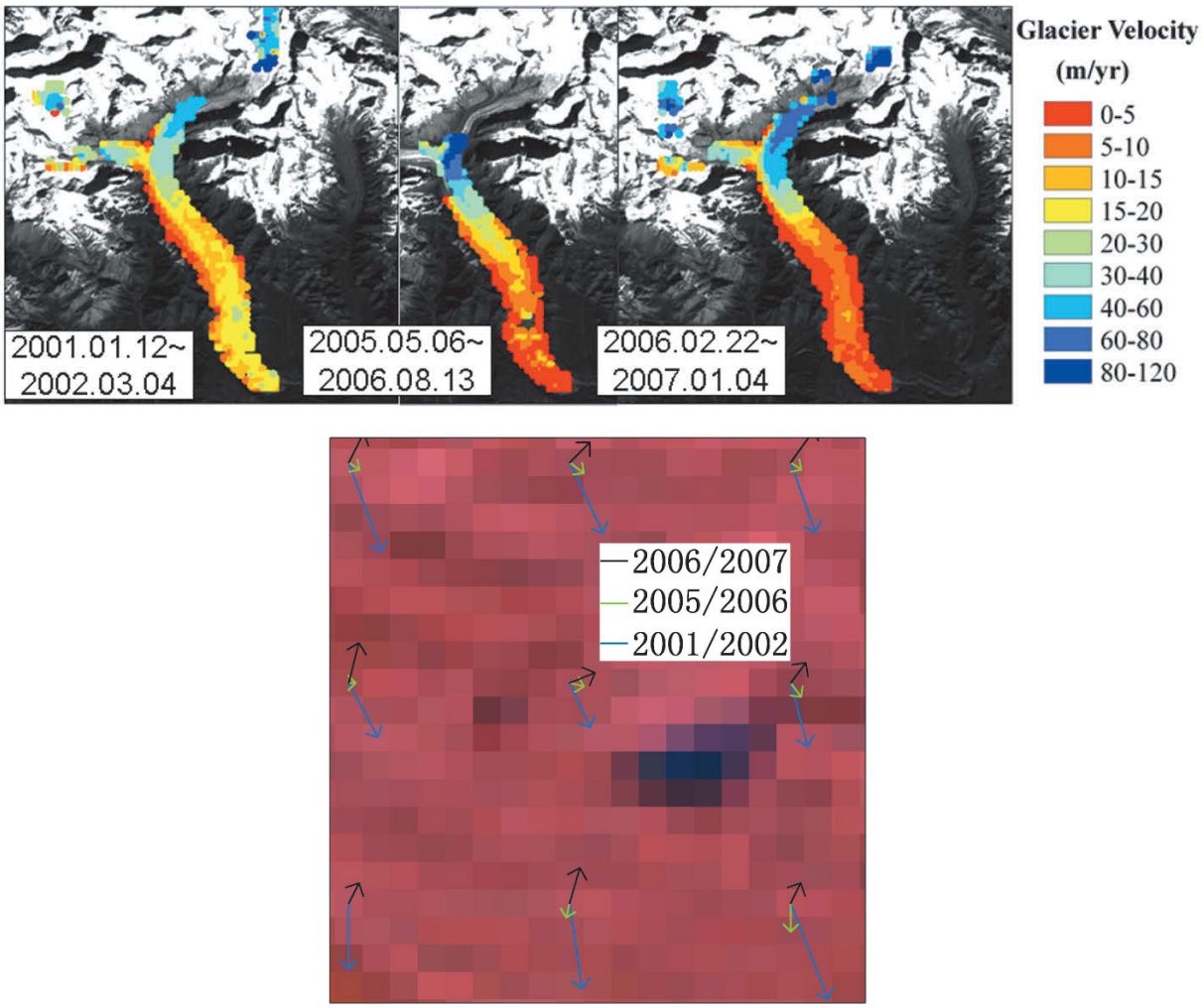

Figure 25.11. Distributions of annual flow velocities of Koxkar Glacier during three phases between 2001 and 2006 (Xu et al. 2011).

The surface velocity field of Koxkar Glacier on the Tomur Peak in the Tianshan Mountains, northwest China, was calculated using the COSI-Corr (Co-registration of Optically Sensed Images and Correlation) software package and ASTER images (Leprince et al. 2007, Xu et al. 2011). Three pairs of ASTER images acquired 2001-01-12/2002-03-04, 2005-05-06/2006-08-13, 2006-02-22/2007-01-04 were used for velocity mapping. Velocities observed by D-GPS (based on 54 stacks) were used for accuracy assessment of velocities extracted from the ASTER images. A mean absolute error of 3.1 m yr^{-1} (11.9%) was obtained. It was found that the glacier was moving fastest near the center and then slowed at both lateral margins. Along a longitudinal profile, the ice velocity increased from the accumulation area to the equilibrium zone, then decreased toward the glacier terminus (Fig. 25.11). The maximum velocity was 117.9 m yr^{-1} at 4,500 m (a.s.l.), while the minimum was 1.3 m yr^{-1} at the glacier terminus and lateral margin in 2006/2007. Glacier speed changed rapidly from 2001 to 2007 in the terminal area (Fig. 25.11).

25.7 SPECIAL TOPICS: HYDROLOGICAL ASPECTS OF CHINESE GLACIER DYNAMICS

25.7.1 Special Topic 1: glacier hazards in the Upper Yalung Zangbo River basin, China

Glacier lakes are widespread and glacier lake outburst flood (GLOF) hazards are among the most serious natural disasters in western China. Between

Table 25.4. Change in ice elevation in the two glaciers since 1956.

Glacier	*Number of pixels in the DEM*	*Period*	*Change in ice elevation*		*Change in volume*
			(m)	(m yr^{-1})	($*10^7$ m^3)
5Y432A1	4,938				
	1,598	1956–1977	-6.8 ± 11	-0.32 ± 0.52	-0.98 ± 1.35
	1,598	1977–2007	-12.7 ± 2	-0.42 ± 0.06	-1.83 ± 0.27
	1,598	1956–2007	-20.2 ± 11	-0.40 ± 0.22	-2.91 ± 1.35
5Y432A5	1,895				
	715	1956–1977	-1.8 ± 11	-0.09 ± 0.52	-0.12 ± 0.55
	715	1977–2007	-15.7 ± 2	-0.52 ± 0.06	-1.00 ± 0.12
	715	1956–2007	-16.9 ± 11	-0.33 ± 0.22	-1.08 ± 0.55

1930 and 2010, many GLOFs were identified or documented as shown in Table 25.5 in the TP. Some historical GLOFs and the general picture of GLOF hazards in the region are described by Cheng et al. (2008). In the Chinese Himalaya, there are 143 potentially dangerous glacier lakes and six indices have been set up to classify and identify them (Wang et al. 2009a). Moreover, moraine-dammed lakes in the Himalaya have been known to form and enlarge due to glacier retreat and increased meltwater availability under climatic warming (Ng et al. 2007). In this section, we give a brief introduction to the monitoring of glacier lakes in the upper reaches of the Yalung Zangbo River, which are mainly distributed on the northern slopes of the Himalaya and the southern slopes of the Nyainqentanglha Mountains.

25.7.1.1 Pumqu Basin

According to catalogued data, there are 229 glacier lakes in the Pumqu Basin (Fig. 25.12), with a total area of 46.75 km^2 and estimated water reserves of 1.23 km^3. These lakes are of several types: cirque lakes, end moraine–dammed lakes, trough valley lakes, and blocking lakes. The most numerous and largest in area are associated with end moraine–dammed lakes, which normally develop in the inner side of remnant moraine ridges from the Little Ice Age (Anon. 1988).

Since the 1940s there have been five GLOFs in the Pumqu River basin (Table 25.5). According to Che et al. (2004), the number of glacier lakes in the Pumqu River basin has reduced to 225. Integrated assessment indicates that 24 glacier lakes are potential candidates for GLOFs. According to Wang et al. (2009b) and Yao et al. (2010), both Longbasaba Lake and Pida Lake in the Pumqu River basin remain at high risk of failure; GLOFs from Longbasaba and Pida Lakes could last for 5.5 hours and have a peak discharge of about $3–5 \times 10^4$ m^3/s at about 1.8 hours into the GLOF.

25.7.1.2 Poiqu Basin

In the Poiqu Basin (Fig. 25.12), there are 45 glacier lakes with a total area of 12.31 km^2 and estimated water reserves of 0.39 km^3. There have been four GLOFs from three glacier lakes in the basin since the 1940s (Table 25.5).

25.7.1.3 Palongzangbu River basin

The Palongzangbu River is closely associated with maritime monsoonal glaciers in China (Fig. 25.12), covering as it does a total area of 638.42 km^2. There is a contiguous distribution of glaciers in the source regions of the Lequzangbu and Boduinzangbu Rivers, covering a total area of 3,588.8 km^2. Based on topographic maps published in 1970 and Landsat TM images in the 1990s and 2000s, there are about 732 glacier lakes in the Palongzangbu River basin. Of these, 142 lakes covering a total area of 10.36 km^2 formed between 1970 and 2000. Analysis shows that 493 of the 732 glacier lakes, covering a total area of 80.79 km^2 in the 1970s, shrank between 1970 and 2000, but enlarged by 9.1% between 1990 and 2000 (Wang et al. 2008).

Moraine-dammed Midui Lake, lying in the middle reaches of Midui Gully in the Palongzangbu River basin burst through its moraine at 23:30 hours on July 15, 1988. Maximum flood discharge is estimated to have been 1,270 m^3/s, flood peak duration greater than 30 minutes, recession duration about 13 hours, and total flood volume of water about $5.4 * 10^6$ m^3 (Li and You, 1992).

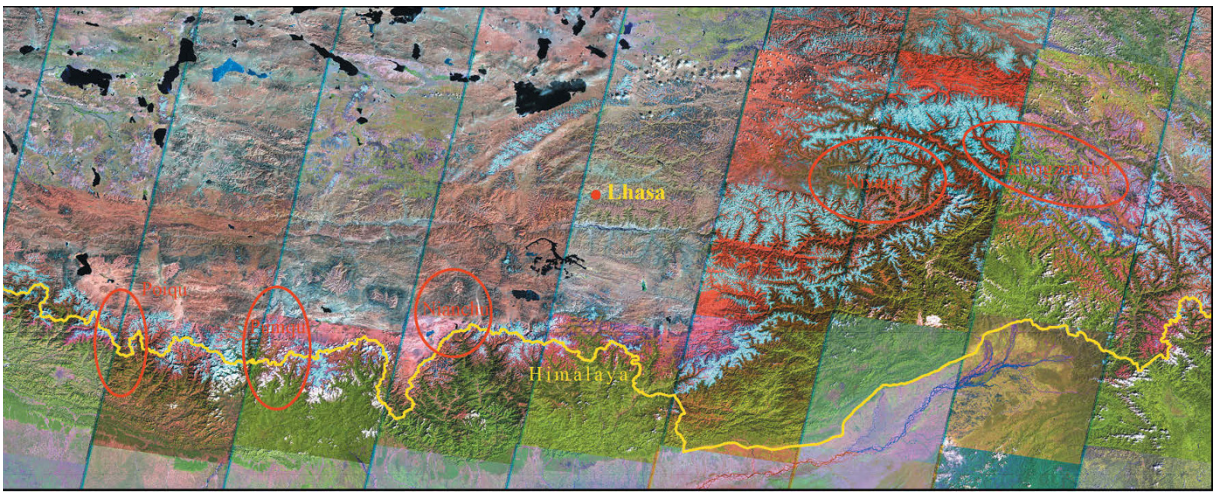

Figure 25.12. Map of basins (red ellipses) in the southern Tibetan Plateau region. Figure can also be viewed as Online Supplement 25.5.

25.7.1.4 Niyang River basin

In the Niyang River basin (Fig. 25.12) there are about 1,089 glacier lakes. In 1970, the total area covered by glacier lakes in the river basin was about 68.46 km^2. Between 1970 and 2000, 34 additional glacier lakes had developed covering a total area of about 1.37 km^2; however, 174 glacier lakes disappeared during the same period (Wang et al. 2008).

25.7.1.5 Nianchu River basin

In the Nianchu River basin there are 49 moraine-dammed lakes (Fig. 25.12), 5 of which are potentially dangerous. The latter occupy a combined area of 3.52 km^2 (Wang et al. 2003a, 2009a). Between 1990 and 2005 glacial lakes expanded by 9.9% in area, possibly the result of accelerated glacier retreat; meanwhile the increased meltwater may have generated new lakes and led to the expansion of existing lakes (Zhou et al. 2009a). In 1954, Zengwanghco Lake, a glacial lake located in the headwaters of the river, flooded and wreaked financial havoc in the lower reaches of the river.

25.7.2 Special Topic 2: glacier water resources in western China provinces

The glaciers in China provide a large quantity of meltwater to several large rivers, such as the Ertix, upper reaches of the Ob, Yellow, Yangtze, Lancang (upper reaches of the Mekong), Nujiang, and Ganges, as well as many internal rivers in arid northwest China. Yang Zhenniang (1991) combined the glacier runoff method, runoff temperature method, and the comparative experiment method, to extrapolate runoff estimates based on observed data in representative mountainous regions and in western China. Glacier runoff is estimated to be between 563.3 and 615.7×10^8 m^3 across China (Yang Zhenniang 1991, Kang et al. 2000, 2009). Note that glacier runoff is the main water resource for internal rivers. Fig. 25.13 shows glacier contribution to water resources as measured at the main hydrological stations of rivers in West China. From this it is recognized that over 38% of water entering the Tarim Basin is glacier runoff.

25.7.2.1 The influence of glacier change on water resources

An observational program at Glacier No. 1, the source of the Urumqi River, at the Tianshan Glacier Station started in 1959 (Xie and Guangwen 1965) and still continues to this day despite a number of interruptions between 1967 and 1979. Long-term climate and glacier records collected during 1959–2004 in the source region of the Urumqi River in the Tianshan Mountains of China show that summer temperature and annual precipitation near the glacier increased by 0.8°C and 87 mm (19%), respectively, during the study period. The glacier continuously retreated from 1962 to 2003, at the end of which period cumulative mass balance was 20% of glacier volume and glacier surface altitude had dropped by −10.032 m. Annual basin runoff significantly increased by 413 mm or 62% during 1980–2003 due to precipitation increase and

Table 25.5. Glacier lakes with outburst history.

No.	*Glacier lake*	*Date*	*Location*		*Basin*	*Damage*
			Latitude	*Longitude*		
1	Tara Co	August 28, 1935	28.29	83.13	Poiqu	Debris flooded 667 hm^2 (667 hectares = 6.7 km^2) of wheat fields
2	Qubixiama Co	July 10, 1940	27.85	88.92	Kangbuqu	A street in Yadong County was flooded and some buildings were damaged
3	Sangwang Co	July 16, 1954	28.24	90.10	Nyangqu River	The flood and debris flow killed 691 people and 8,679 livestock, destroyed 170 villages in Gyantse County and Bainang County. It was the worst GLOF disaster on record in Tibet
4	Lure Co	1950s	28.27	90.59	Zharixiongqu	—
5	Cirenma Co	1964 July 11, 1984	28.07	86.06	Poiqu	The debris flow killed 200 people, destroyed the China–Nepal Friendship Bridge and other buildings along the river, and caused serious damage downstream at the Sun Koshi hydropower station
6	Longda Co	August 25, 1964	28.62	85.35	Jilongzangbo	The outburst flood washed away a huge amount of sediment, which created a debris blockage 800 m along the river
7	Gelhaipu Co	September 21, 1964	27.96	87.81	Pumqu	Highway damaged; 12 timber trucks washed away; unspecified number of human casualties
8	Damenhai Co	September 26, 1964	29.87	93.04	Yarlungzangbo	The debris flow damaged villages and blocked the Niyang River for 16 hours
9	Aya Co	August 15, 1968 August 17, 1969 August 18, 1970	28.35	86.49	Pumqu	Roads and one concrete bridge damaged as far as 40 km away
10	Poge Co	July 23, 1972	31.73	94.73	Nujiang River	The flood destroyed a few minor bridges
11	Boge Lake	July 6, 1974	31.86	94.76	Nujiang River	The road from the town of Heihe to Changdu was destroyed and some wooden bridges were swept away
12	Zhari Co	June 24, 1981	28.30	90.61	Zharixiongqu	The flood destroyed infrastructure: mills, hydropower station, bridges, and houses

13	Yindapu Co	August 27, 1982	27.95	87.91	Pumqu	Over 1,600 head of livestock were lost, 20 hm^2 of cultivated fields were flooded and houses in eight villages suffered different degrees of damage
14	Guangxie Co	July 15, 1988	29.46	96.50	Palongzangbo	The flood killed 5 people and 50 livestock, destroyed 18 bridges and disrupted the Sichuan–Tibet Highway for nearly half a year. The economic loss was about CNY 0.1 billion.
15	Xiaga Lake	May 26, 1995	28.80	91.94	Yalong River	The flood covered 16 hm^2 of cultivated land, 67 hm^2 of pasture, and destroyed 22 bridges
16	Zhanapo Lake	June 7, 1995	28.66	85.37	Jilongzangbo	The debris destroyed a 28 km stretch of a highway
17	Longjiu Co	August 6, 2000	28.24	89.69	Yarlungzangbo	—
18	Jialong Co	May 23, 2002 June 29, 2002	28.21	85.85	Poiqu	A concrete bridge was destroyed by debris. The China–Nepal road and a new hydropower station were partially damaged. The overall economic loss was about CNY 7.5 million
19	Dega Co	September 18, 2002	28.33	90.67	Zharixiongqu	The flood killed 9 people, destroyed 18 bridges, and inundated 190.8 hm^2 of farmland. The economic loss was about CNY 30 million.
20	Lang Co	August 10, 2007	27.83	91.81	Yarlungzangbo	The frontier defense inspection station and an iron bridge were destroyed
21	Zhemai Co	July 3, 2009	28.01	92.34	Yarlungzangbo	The flood destroyed a 3 km stretch of a road, 3 culvert bridges, and 4 minor bridges
22	Cuoga Lake	July 29, 2009	30.83	94.00	Yarlungzangbo	The flood killed 2 people, destroyed a 27 km stretch of road, 2 iron bridges, and 4 concrete bridges. Additionally, 2 cars and 17 motorcycles were swept away
23	Geiqu Lake	2010	27.95	87.99	Pumqu	The road leading to Longbasaba Lake was destroyed and a culvert bridge was damaged
24	Ranzeria Co	July 5, 2013	30.47	93.53	Yarlungzangbo	49 houses were completely destroyed, some people and livestock were killed, and a concrete bridge was damaged. The total economic loss was about CNY 0.25 billion

Adapted from Xu and Feng Qinghua (1989) and Yao et al. (2014).

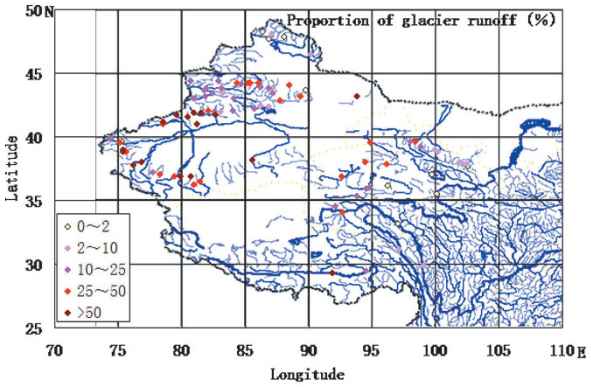

Figure 25.13. The proportion of glacier runoff in water at the main hydrological stations in the rivers in West China (Ye et al. 2005). Figure can also be viewed as Online Supplement 25.6.

enhanced glacier melt caused by increased summer climate warming. Two thirds of the increase in glacier runoff (close to a quarter of total recent annual flow discharge) was the result of glacier mass loss (Ye et al. 2005). This is among the highest runoff percentages of major rivers due to the negative mass balance of glaciers (see Section 25.7.2.3 for the highest).

A comparative method study, using repeat aerial photogrammetric mapping to monitor variation in glacier size and morphological factors, has been undertaken in the drainage area of the Urumqi River. The study results show that higher accuracy can be achieved in the determination of glacier length, area, and ice storage variation by applying more precise datasets (e.g., aerial photos versus satellite imagery). Such datasets can also be of help in monitoring regional glacier variation. Measurement data show that all 155 glaciers in the drainage area of the Urumqi River retreated during the period 1964–1992, with an average retreat of 12.4% and an average rate of glacier area change of −13.8%. Mean glacier surface altitude dropped 5.8 m, equivalent to a loss of 15.8% of ice storage (Chen et al. 1996).

25.7.2.2 Glacier volume change

Degree-day factors are the key parameters of degree-day models and clearly vary regionally (Zhang et al. 2006b). The degree-day meltwater model has been verified for use in the Tarim Basin and can be employed to estimate glacier runoff. Estimates show the positive anomaly in stream runoff of the Tailan River (one of tributaries of the Tarim Basin) can be partly attributed to the increase in glacier runoff (amounting for one third of stream discharge). Rough estimates using observed average ablation at the termini of 15 glaciers in China verify that mass loss calculated by the relationship between glacier area and volume is reasonable (Liu et al. 2006).

Change in total ice volume has been estimated from the shrinkage area of glaciers in the basin using a verified glacier area–volume relationship for the Tarim Basin. Glacier area change has been surveyed using recent remote-sensing data, and compared with the Chinese Glacier Inventory (Shi et al. 2005), which is based on aerial photos taken from the late 1950s to the early 1980s and large-scale topographic maps. There are 3,081 monitored glaciers in the Tarim Basin (representing 50.3% of total glacial area and 26.4% of the total number of glaciers in the Tarim Basin). The ice volume of the glaciers monitored generally decreased by 35.5 km^3, or 319.3×10^8 m^3 (water equivalent) (assuming an ice density of 900 kg m^{-3}), which was estimated from the area–volume relationship and glacier area change. This means glacier mass loss contributed about 5% of annual discharge into the Tarim Basin (Liu et al. 2006). The results of Yao et al. (2004) also show that glacial retreat in the 1990s caused a 5.5% increase in river runoff in northwest China. According to estimates by Gao et al. (2010) using the degree-day meltwater model, mass balance in the Tarim River basin reduced by −6.4 m (−139.2 mm yr^{-1}) between 1961 and 2006 and annual glacier meltwater runoff was 180.40×10^8 m^3, contributing about 41.5% of annual river runoff. The results show that glacial retreat between 1991 and 2006 was responsible for an increase of 85.7% in annual river runoff, relative to annual river runoff between 1961 and 1990 in the Tarim River basin.

25.7.2.3 Potential influences of future glacier change

Projections of glacier change over China have been made using regional glacier change results since the Little Ice Age (Shi and Liu 2000). The results indicate that China's glacier area would reduce by 12, 28, and 45% by 2030, 2070, and 2100, respectively, if air temperature increased by 0.4–1.2, 1.2–2.7, and 2.1–4.0°C at the same time. Degree-day model results show that a 1°C increase of air temperature would lead to an increase in glacier runoff of about 60–80% in the Yili River, Tianshan (Ye et al. 2003). Based on climate-change scenarios, glacier runoff in the Yangtze River Source Region (YRSR) by 2050

is expected to increase by 29.2% (IPCC Scenario A2) and 29.8% (IPCC Scenario B1), compared with the climatic normal period 1961–1990 (Liu et al. 2009).

25.8 SUMMARY AND FUTURE PROSPECTS

In summary, the overall trend for glaciers in western China over the last five decades has been one of retreat; however, regional differences exist. These we attribute to the different dynamical responses of glaciers as a function of their different sizes and physical properties along with regional differences in climate change. Surface elevation lowering may be larger than expected or estimated by the empirical relation for ice volume change, as shown by ASTER DEM extraction measurements and DGPS survey of ablation on a monitored glacier. Experiments on how best to estimate the surface velocity of glaciers indicate the potential for widespread application of remote-sensing techniques to monitor glacier movements in the high mountains of western China.

Glacier recession is the key factor involved in water resource variability in the arid river systems of northwest China. The recent increase in discharge from these rivers may be partially related to glacial runoff increase caused by loss of ice during glacier retreat. Although the glaciers that we (and others) have monitored account for only 10% of the number and 24% of the total area of glaciers in China, our results may be extrapolated to infer glacier changes in China's diverse mountain regions. However, a more comprehensive glacier monitoring effort is needed as there are regions where glacier change has yet to be assessed. In addition, to determine ice volume changes and to validate the results requires higher resolution images with stereoscopic capability, involving such techniques as SPOT-5, SAR/InSAR, and laser altimetry. Furthermore, field investigations must be intensified and modeling techniques applied to typical glacierized watersheds to better understand the processes involved in glacial runoff.

25.9 ACKNOWLEDGMENTS

ASTER data courtesy of NASA/GSFC/METI/Japan Space Systems, the U.S./Japan ASTER Science Team, and the GLIMS project.

25.10 REFERENCES

Anon. (1988) *Sino-Nepalese Investigation of Glacier Lake Outburst Floods in the Himalayas* (report on first expedition to glaciers and glacier lakes in the Pumqu and Poiqu River Basins, Tibet, China), Science Press, Beijing.

Bahr, D.B., Meier, M.F., and Peckham, S.D. (1997) The physical basis of glacier volume-area scaling. *Journal of Geophysical Research*, **102**, 20355–20362.

Berthier, E., Vadon, H., Baratoux, D., Arnaud, Y., Vincent, C., Feigl, K.L., Rémy, F., and Legrésy, B. (2005) Surface motion of mountain glaciers derived from satellite optical imagery. *Remote Sensing of Environment*, **95**(1), 14–28.

Che Tao, Jin Rui, Li Xin, and Wu Lizong (2004) Glacial lakes variation and the potentially dangerous glacial lakes in the Pumqu Basin of Tibet during the last two decades. *Journal of Glaciology and Geocryology*, **26**(4), 397–402 [in Chinese with English abstract].

Chen Jianming, Liu Chaohai, and Jin Mingxie (1996) Application of the repeated aerial photogrammetry to monitoring glacier variation in the drainage area of the Urumqi River. *Journal of Glaciology and Geocryology*, **18**(4), 331–336 [in Mandarin with English abstract].

Cheng Zunlan, Zhu Pingyi, Dang Chao, and Liu Jingjing (2008) Hazards of debris flow due to glacier-lake outburst in southeastern Tibet. *Journal of Glaciology and Geocryology*, **30**(6), 954–959 [in Chinese].

Ding Yongjian, Liu Shiyin, Li Jing, and Shangguan Donghui (2006) The retreat of glaciers in response to recent climate warming in western China. *Annals of Glaciology*, **43**, 97–105.

Dyurgerov, M., Meier, M., and Armstrong, R. (Eds.) (2002) *Glacier Mass Balance and Regime: Data of Measurements and Analysis* (INSTAAR Occasional Paper No. 55), Institute of Arctic and Alpine Research. University of Colorado, Boulder, CO.

Gao Xin, Ye Baisheng, Zhang Shiqiang, Qiao Chengjun, and Zhang Xiaowen (2010) Glacier runoff variation and its influence on river runoff during 1961–2006 in the Tarim River Basin, China. *Science China, Series D: Earth Science*, **40**(5), 654–665 [in Mandarin].

Gardelle, J., Berthier, E., and Arnaud, Y. (2012) Slight mass gain of Karakoram glaciers in the early twenty-first century. *Nature Geoscience*, doi: 10.1038/NGEO1450.

Hirano, A., Welch, R., and Lang, H. (2003) Mapping from ASTER stereo image data: DEM validation and accuracy assessment. *Journal of Photogrammetry and Remote Sensing*, **57**, 356–370.

Jiang Zongli, Liu Shiyin, and Han Haidong (2011a) Analyzing mountain glacier surface velocities using SAR data. *Remote Sensing Technology and Application*, **26**(5): 640–646.

Jiang Zongli, Liu Shiyin, and Peters, J. (2011b) Analyzing Yengisogat Glacier surface velocities with ALOS PALSAR data feature-tracking, Karakoram, China. *Environmental Earth Sciences*, doi: 10.1007/s12665-012-1563-9.

Jin Rui, Che Tao, Li Xin, and Wu Lizong (2004) Glacier variation in the Pumqu Basin derived from remote sensing data and GIS technique. *Journal of Glaciology and Geocryology*, **26**(3): 261–266 [in Mandarin].

Joughin, I., Kwok, R., and Fahnestock, M. (1996) Estimation of ice-sheet motion using satellite radar interferometry. *Journal of Glaciology*, **42**(142), 564–575.

Kääb, A. (2005) Combination of SRTM3 and repeat ASTER data for deriving alpine glacier flow velocities in the Bhutan Himalaya. *Remote Sensing of Environment*, **94**, 463–474.

Kääb, A., Huggel, C., Paul, F., Wessels, R., Raup, B., Kieffer, H., and Kargel, J. (2003) Glacier monitoring from ASTER imagery: Accuracy and applications. *EARSeL eProceedings*, **2**, 43–53.

Kang Ersi, Yang Zhengniang, and Lai Zuming (2000) Glacier and snow meltwater and runoff in mountains. In: Shi Yafeng (Ed.), *Glacier and Environments in China*, Science Press, Beijing, pp. 190–233.

Kang Ersi, Liu Chaohai, Xie Zichu, Li Xin, and Shen Yongping (2009) Assessment of glacier water resources based on the Glacier Inventory of China. *Annals of Glaciology*, **50**(53), 104–110.

Leprince, S., Ayoub, F., Klinger, Y., and Avouac, J.P. (2007) Co-registration of Optically Sensed Images and Correlation (COSI-Corr): An operational methodology for ground deformation measurements. Paper presented at *IEEE International Geoscience and Remote Sensing Symposium (IGARSS 2007), Barcelona, July 2007*.

Li Deji and You Yong (1992) Bursting of the Midi moraine lake in Bomi, Xizang. *Mountain Research*, **10**(4), 219–224 [in Mandarin with English abstract].

Liu Chaohai, Wang Zongtai, Ding Liangfu (Eds.) (2001) *Glacier Inventory of China IV, Revised Edition: Pamirs* (drainage basins of Kaxgar River and others), Gansu Culture Publishing House, Lanzhou, China [in Mandarin].

Liu Chaohai, Xie Zichu, and Liu Shiyin (2002a) Glacial water resources and their change. In: E. Kang, G. Cheng, and Z. Dong (Eds.), *Glacier-snow Water Resources and Mountain Runoff in the Arid Area of Northwest China*, Science Press, Beijing, pp. 14–51 [in Mandarin].

Liu Shiyin, Lu Anxin, Ding Yongjian, Yao Tandong, Ding Liangfu, Li Gang, and Hooke, R. (2002b) Glacier fluctuations and inferred climate changes in the Anyemaqen Mountains in the source area of the Yellow River. *Journal of Glaciology and Geocryology*, **24**(6), 701–707 [in Mandarin].

Liu Shiyin, Sun Wenxin, Shen Yongping, and Li Gang (2003) Glacier changes since the Little Ice Age maximum in the western Qilian Shan, northwest China, and consequences of glacier runoff for water supply. *Journal of Glaciology*, **49**(164), 117–124.

Liu Shiyin, Shangguan Donghui, Ding Yongjian, Zhang Yong, Wang Jian, Xie Changwei, Ding Liangfu, and Li Gang (2004) Variation of glaciers studied on the basis of RS and GIS: A reassessment of the changes of the Xinqingfeng and Malan Ice Caps in the Northern Tibetan Plateau. *Journal of Glaciology and Geocryology*, **26**(3), 244–252 [in Mandarin].

Liu Shiyin, Shangguan Donghui, Ding Yongjian, Han Haidong, Xie Changwei, Zhang Yong, Li Jing, Wang Jian, and Li Gang (2005) Glacier changes since the early 20th century in the Gangrigabu Mountains, Southeast Tibetan Plateau. *Journal of Glaciology and Geocryology*, **27**(1), 55–63 [in Mandarin].

Liu Shiyin, Ding Yongjian, Shangguan Donghui, Zhang Yong, Li Jing, Han Haidong, Wang Jian, and Xie Changwei (2006) Glacier retreat as a result of climate warming and increased precipitation in the Tarim river basin, northwest China. *Annals of Glaciology*, **43**, 91–96.

Liu Shiyin, Zhang Yong, Zhang Yingsong, and Ding Yongjian (2009) Estimation of glacier runoff and future trends in the Yangtze River source region, China. *Journal of Glaciology*, **55**(190), 353–362.

Lu Anxin, Yao Tandong, Liu Shiyin, Ding Liangfu, and Li Gang (2002) Glacier change in the Geladandong area of the Tibetan Plateau monitored by remote sensing. *Journal of Glaciology and Geocryology*, **24**(5), 559–562 [in Mandarin with English abstract].

Luckman, A., Quincey, D., and Bevan, S. (2007) The potential of satellite radar interferometry and feature tracking for monitoring flow rates of Himalayan glaciers. *Remote Sensing of Environment*, **111**(2/3), 172–181.

Mi Desheng and Xie Zichu (2002) *Glacier Inventory of China, Vol. XI: Ganges River* and *Vol. XII: Indus River*, Xi'an Cartographic Publishing House, Xi'an, China.

Ng, F., Liu, S., Mavlyudo, B. et al. (2007) Climatic control on the peak discharge of glacier outburst floods, *Geophysical Research Letters*, **34**, L21503, doi: 10.1029/2007GL031426.

Shangguan Donghui (2007) Glacier changes in Tarim Interior River Basin using 3S. Ph.D. dissertation, Cold and Arid Regions Environmental and Engineering Research Institute, Chinese Academy of Sciences, Beijing, pp. 1–132.

Shangguan Donghui, Liu Shiyin, and Ding Yongjian (2004a) Glacier changes at the head of Yurungkax River in the West Kunlun Mountains in the past 32 years. *Acta Geographica Sinica*, **59**(6), 855–862 [in Mandarin].

Shangguan Donghui, Liu Shiyin, and Ding Yongjian (2004b) Monitoring results of glacier changes in China

Karakorum and Muztag Ata–Konggur Mountains by remote sensing. *Journal of Glaciology and Geocryology*, **26**(3), 374–375 [in Mandarin].

Shangguan Donghui, Liu Shiyin, Ding Yongjian, Ding Liangfu, Xiong Libing, Cai Dihua, Li Gang, Lu Anxin, Zhang Shiqiang, and Zhang Yong (2006) Monitoring the glacier changes in the Muztag Ata and Konggur mountains, east Pamirs, based on Chinese Glacier Inventory and recent satellite imagery. *Annals of Glaciology*, **43**, 79–85.

Shi Yafeng, and Bai Zhongyuan (1988) Geomorphological and climate settings of glacier development and the snow distribution in western China. In: Shi Yafeng (Ed.), *An Introduction of Glaciers in China*. Science Press, Beijing, pp. 12–28 [in Mandarin].

Shi Yafeng, and Liu Shiyin (2000) Estimation of the response of glaciers in China to the global warming in the 21st century. *Chinese Sciences Bulletin*, **45**(4), 434–438 [in Mandarin].

Shi Yanfeng, Liu Chaohai, Wang Zongtai, Liu Shiyin, and Ye Baisheng (2005) *A Concise China Glacier Inventory*, Shanghai Science Popularization Press, Shanghai [in Mandarin].

Su Zhen, and Shi Yafeng (2000) Response of monsoonal temperate glaciers in China to global warming since the Little Ice Age. *Journal of Glaciology and Geocryology*, **22**(3), 223–229 [in Mandarin with English summary].

Wang Ninglian, and Ding Liangfu (2002) Study on the glacier variation in Bujiagangri section of the east Tanggula range since the Little Ice Age. *Journal of Glaciology and Geocryology*, **24**(3), 234–244 [in Mandarin].

Wang Tiefeng, Liu Zhirong, Xia Chuanqing et al. (2003a) Study of the glacial lakes in the Nianchu River Basin, Tibet. *Journal of Glaciology and Geocryology*, **25**(2), 344–348 [in Mandarin with English abstract].

Wang Jiexian, Wang Jun, and Lu Caiping (2003b) Problem of coordinate transformation between WGS-84 and BEIJING 54. *Journal of Geodesy and Geodynamics*, **23**(3), 70–73 [in Mandarin].

Wang Lihong, Zhao Jie, Lu Anxin, Zhang Chunwen, and Zhang Huawei (2008) The study of lake variation using remote sensing near S301 Highway in Tibetan Plateau from 1970 to 2000. *Remote Sensing Technology and Application*, **23**(6), 658–661.

Wang Xin, Liu Shiyin, Guo Wanqin, and Xu Junli (2009b) Assessment and simulation of glacier lake outburst floods for Longbasaba and Pida Lakes, China. *Mountain Research and Development*, **28**(3/4), 310–317.

Wang Xin, Liu Shiyin, Guo Wanqin, Yu Pengchun, and Xu Junli (2009a) Hazard assessment of moraine-dammed lake outburst floods in the Himalayas, China. *Acta Geographica Sinica*, **64**(7), 782–790 [in Mandarin with English abstract].

Wang Zongtai (1991) The Little Ice Age of northwest China. *Journal of Arid Land Resources and Environment*, **5**(3), 64–74 [in Mandarin with English abstract].

Xie Zichu, and Ge Guangwen (1965) The accumulation, ablation, and mass balance on Glacier No. 1 in the headwaters of the Urumqi River, Tianshan, *Studies on Glaciers and Hydrology in the Urumqi River, Tianshan*, Science Press, Beijing, pp. 14–24.

Xu Daoming, and Feng Qinghua (1989) Dangerous glacial lake and outburst features in Xizang Himalayas. *Acta Geographica Sinica*, **44**(3), 343–352.

Xu Junli, Zhang Shiqiang, Han Haidong, Liu Shiyin, and Zhang Yingsong (2011) Changes of the surface velocity of Koxkar Glacier interpreted from remote sensing data, Tianshan Mountains. *Journal of Glaciology and Geocryology*, **33**(2), 268–275 [in Mandarin with English abstract].

Yang Hui'an, and An Ruizhen (Eds.) (1989) *Glacier Inventory of China, V: Karakorum Mountains—Drainage Basin of the Yarkant River*, Science Press, Beijing [in Mandarin].

Yang Zhenniang (1991) *Glacier Water Resources in China*, Gansu Scientific and Technological Press, Lanzhou, China, pp. 81–152.

Yang Zhenniang, and Zeng Qunzhu (Eds.) (2001) *Glacier Hydrology*, Chongqing Press, Chongqing, China [in Mandarin].

Yao Tandong, Wang Youqing, Liu Shiyin et al. (2004) Recent glacial retreat in High Asia in China and its impact on water resource in Northwest China. *Science in China, Series D: Earth Sciences*, **47**(12), 1065–1075.

Yao Xiaojun, Liu Shiyin, and Wei Junfeng (2010) Reservoir capacity calculation and variation of moraine-dammed lakes in the north Himalayas: A case study of Longbasaba Lake. *Acta Geographica Sinica*, **65**(11), 1381–1390 [in Mandarin with English abstract].

Yao Xiaojun, Liu Shiyin, and Sun Meiping (2014) Study on the glacial lake outburst flood events in Tibet since 20th century. *Journal of Natural Resources*, accepted.

Ye Baisheng, Ding Yongjian, and Liu Fengjing (2003) Responses of various scale mountain valley glaciers and corresponding runoffs to climatic change. *Journal of Glaciology*, **49**(164), 1–7.

Ye Baisheng, Yang Daqing, Jiao Keqin et al. (2005) The Urumqi River source Glacier No. 1, Tianshan, China: Changes over the past 45 years. *Geophysical Research Letters*, **32**, L21504, doi: 10.1029/2005GL024178.

Zebker, H.A., Werner, C.L. et al. (1994) Accuracy of topographic maps derived from ERS-1 interferometric radar. *IEEE Transactions on Geoscience and Remote Sensing*, **32**(4), 823–836.

Zhang Xiangsong (1980) Recent variations of the Insukati Glacier and adjacent glaciers in the Karakoram Mountains. *Journal of Glaciology and Geocryology*, **2**(3), 12–16 [in Mandarin].

Zhang Yong, Liu Shiyin, Ding Yongjian et al. (2006a) Preliminary study of mass balance on the Koxkar Glacier on the south slope of Tianshan Mountains. *Journal of Glaciology and Geocryology*, **28**(4), 477–484 [in Mandarin].

Zhang Yong, Liu Shiyin, and Ding Yongjian (2006b) Spatial variation of degree-day factors on the observed glaciers in western China. *Acta Geographica Sinica*, **61**(1), 89–98 [in Mandarin].

Zhou Jianmin, and Li Zhen (2011) Estimating the motion of Dongkemadi Glacier in Qinghai–Tibet Plateau using differential SAR interferometry with corner reflectors. Paper presented at *IGARSS, 2011, Vancouver, BC, Canada*, pp. 3183–3186.

Zhou Caiping, Yang Wenbin, Wu Liang et al. (2009a) Glacier changes from a new inventory, Nianchu river basin, Tibetan Plateau. *Annals of Glaciology*, **50**(53), 87–92.

Zhou Jianmin, Li Zhen, and Li Xinwu (2009b) Research on rules of the valley glacier motion in western China based on ALOS/PALSAR interferometry. *Acta Geodaetica et Cartographica Sinica*, **38**(4), 341–347.